RESEARCH ARTICLE

Key Points:

- The majority of the first cloud-to-ground flashes are preceded by intracloud lightning
- Initial positive differential reflectivity anomaly is present aloft, associated with supercooled raindrops
- Reduced differential reflectivity is present before and during the time of the initial lightning flash

Correspondence to:
E. V. Mattos,
enrique.vmattos@gmail.com

Electrification life cycle of incipient thunderstorms

Enrique V. Mattos[1,2] (ID), **Luiz A. T. Machado[1]** (ID), **Earle R. Williams[3]** (ID), **Steven J. Goodman[4]** (ID), **Richard J. Blakeslee[5]** (ID), and **Jeffrey C. Bailey[6]**

[1]Centro de Previsão de Tempo e Estudos Climáticos, Instituto Nacional de Pesquisas Espaciais, Cachoeira Paulista, São Paulo, Brazil, [2]Now at Instituto de Recursos Naturais, Universidade Federal de Itajubá, Itajubá, Minas Gerais, Brazil, [3]Parsons Laboratory, Massachusetts Institute of Technology, Cambridge, Massachusetts, USA, [4]NOAA/NESDIS/GOES-R Program Office, Greenbelt, Maryland, USA, [5]NASA Marshall Space Flight Center, Huntsville, Alabama, USA, [6]Earth System Science Center, University of Alabama in Huntsville, Huntsville, Alabama, USA

Abstract This work evaluates how clouds evolve to thunderstorms in terms of microphysical characteristics to produce the first intracloud (IC) and cloud-to-ground (CG) lightning flashes. Observations of 46 compact isolated thunderstorms during the 2011/2012 spring-summer in Southeast Brazil with an X-band polarimetric radar and two- and three-dimensional Lightning Location Systems demonstrated key parameters in a cloud's vertical structure that produce the initial electrification and lightning activity. The majority (98%) of the first CG flashes were preceded (by approximately 6 min) by intracloud (IC) lightning. The most important aspect of the observations going into this paper, which came originally from the visual examination of a large number of thunderstorms, is that an initial positive differential reflectivity (Z_{DR}) (associated with supercooled raindrops) evolved to reduced Z_{DR} (and even negative values) in the cloud layer between 0° and to $-15°C$ before and during the time of the initial lightning, suggesting evolution from supercooled raindrops to frozen particles promoting the formation of conical graupel. An enhanced negative specific differential phase (K_{DP}) (down to $-0.5° \text{km}^{-1}$) in the glaciated layer (above $-40°C$) was predominantly observed at the time of the first CG flash, indicating that ice crystals, such as plates and columns, were being vertically aligned by a strong electric field. These results demonstrate that the observations of Z_{DR} evolution in the mixed layer and negative K_{DP} in the upper levels of convective cores may provide useful information on thunderstorm vigor and lightning nowcasting.

1. Introduction

Lightning is recognized as an important atmospheric component; however, the knowledge about the electrification process and life cycle in thunderstorms is still limited. Understanding this process and the thunderstorm life cycle will help develop nowcasting tools and lightning parameterization in numerical weather models. The common aspect provided by experimental simulations and observational studies is that collisions between graupel and small ice crystals inside an environment dominated by supercooled water and strong updrafts is the primary process of thunderstorm electrification [*Reynolds et al.*, 1957; *Takahashi*, 1978]. Cloud microphysical estimations from weather radar have provided a significant improvement in the understanding of hydrometeor characteristics and the production of lightning in thunderstorms [*Workman and Reynolds*, 1949; *Reynolds and Brook*, 1956; *Goodman et al.*, 1988; *Buechler and Goodman*, 1990; *Hondl and Eilts*, 1994; *Jameson et al.*, 1996]. Nevertheless, the understanding on how the clouds evolve, from the first cloud droplets to full thunderstorms and how the first intracloud (IC) lightning and cloud-to-ground (CG) lightning flashes are produced using an large sample of compact and isolated thunderstorms, is still lacking.

Observations provided by single- and dual-polarization radar have shown an organized progression from the first development of supercooled raindrops to the initial electrification [*Workman and Reynolds*, 1949; *Reynolds and Brook*, 1956; *Krehbiel*, 1986; *Goodman et al.*, 1988; *Ramachandran et al.*, 1996; *Jameson et al.*, 1996; *Bringi et al.*, 1997; *López and Aubagnac*, 1997; *Carey and Rutledge*, 2000; *Bruning et al.*, 2007; *MacGorman et al.*, 2008; *Woodard et al.*, 2012; *Mecikalski et al.*, 2015; *Stolzenburg et al.*, 2015]. *Workman and Reynolds* [1949] evaluated the initial electrification in 12 summer storms in New Mexico and reported the occurrence of the first IC lightning approximately 13 min following the first radar echo and coincident with the time that the radar echo begins to descend. Meanwhile, *Reynolds and Brook* [1956] showed that initial electrification in thunderstorms is associated with a rapid vertical development of the initial

radar-precipitation echo. *Goodman et al.* [1988] used polarimetric radar and documented the first IC lightning event approximately 4–6 min after water at the top of a supercooled column froze and radar-inferred graupel particles had formed. On the other hand, *Ramachandran et al.* [1996] analyzed several convective cells within two Florida storms with in situ aircraft and polarimetric radar observations. They observed the first CG lightning 15 min after the first radar echo and after the development of ice phase precipitation via the freezing of supercooled rain within the upper portion of the updraft region, followed by the appearance of an electric field of tens of kilovolts per meter close to the $-6°C$ isotherm. Additionally, *Jameson et al.* [1996] showed that the onset of electrification coincided with the appearance of significant volumes of differential reflectivity (Z_{DR}) above the $-7°C$ level. More recently, *Stolzenburg et al.* [2015] examined the initial electrification of New Mexico thunderstorms and documented the initiation of the first IC flash at temperatures between $-10°$ and $-20°C$ and 5–8.6 min after the earliest deflection of electric field at surface. The authors documented that the initial electrification became evident at the surface after stronger reflectivity Z_H (40 dBZ) developed above the $-5°C$ isotherm, and a rapid growth of the surface electric field was observed after this Z_H extended above the $-15°C$ isotherm. The results suggested also that the radar data with higher time resolution could improve the lead time by 2–7 min in detecting the onset of initial electrification compared with the electric field measurements at the surface.

Indeed, the aforementioned studies show the importance of the regions with larger raindrops above the melting layer (defined as $+Z_{DR}$ columns) for the formation of graupel embryos, that in turn, such mixed-phase hydrometeors (graupel, ice crystals, and supercooled raindrops) are fundamental for the early cloud electrification. $+Z_{DR}$ columns and their vertical extent are well correlated with the updraft intensity [*Hall et al.*, 1980, 1984; *Caylor and Illingworth*, 1987; *Illingworth et al.*, 1987; *Bringi et al.*, 1991; *Herzegh and Jameson*, 1992; *Conway and Zrnić*, 1993; *Ryzhkov et al.*, 1994; *Hubbert et al.*, 1998; *Smith et al.*, 1999; *Picca et al.*, 2010; *Kumjian et al.*, 2012, 2014; *Homeyer and Kumjian*, 2015; *Snyder et al.*, 2015]. The pioneering work presented by *Hall et al.* [1984] documented a narrow column of strong Z_H (~48 dBZ) and positive Z_{DR} (~+2.5 dB) reaching 1.5 km above the melting layer, which was interpreted as supercooled water carried upward by strong updraft. *Illingworth et al.* [1987] also documented positive Z_{DR} (~+3 dB) and moderate Z_H (~30 dBZ) extending up to the $-10°C$ level in developing convective clouds and attributed this observation to a low concentration of large (>4 mm diameter) supercooled raindrops. Their observations suggested also that $+Z_{DR}$ columns persist for less than 10 min with column diameters between 1 and 2 km. The authors argued that such a low concentration of large raindrops could be efficient as hail embryos, growing to large hailstones after the freezing process due to the lack of competition for cloud water. *Hubbert et al.* [1998] evaluated polarimetric radar measurements and ground observations of hail in Colorado and documented that 30–40% of the hailstones contained frozen drop embryos. This result showed the importance of mixed-phase particles in the upper portion of the $+Z_{DR}$ columns for the formation of hail. In addition, *Smith et al.* [1999] evaluated Z_{DR} signatures and linear depolarization ratio (LDR) using 3 cm radar and compared with in situ photographs and shadowgraphs of precipitation particle observations by the T-28 aircraft in a Florida convective storm. $+Z_{DR}$ columns presented large positive Z_{DR} (between +2 and +3 dB) and large LDR (-24 and -30 dB) close to $-10°C$ level, possibly indicating the initial freezing of rain.

More recently, *Homeyer and Kumjian* [2015] analyzed the behavior of the polarimetric signature in three different overshooting convective thunderstorms: organized convection, discrete ordinary convection, and discrete supercell convection. Their results revealed deep columns of highly positive Z_{DR} and specific differential phase (K_{DP}) representing the lofting of liquid hydrometeors within the convective updraft and above the melting level. The condensation and coalescence processes in the updraft regions are the possible response to growth of large drops observed in $+Z_{DR}$ columns [*Illingworth et al.*, 1987]. In addition, *Caylor and Illingworth* [1987] suggested that ultragiant nuclei could also contribute to the growth of such large drops. *Kumjian et al.* [2014] proposed that initial cloud droplets grow via vapor diffusion and coalescence to the size of small raindrops that fall out in weaker updrafts. Some of these small raindrops are recirculated into the updraft and grow by coalescence with other raindrops until they reach large size and start to fall. Other raindrops are lofted into strong updrafts and grow at a lower rate. These regions are a probable source area for graupel embryos, produced by raindrops frozen inside those columns, which are fundamental for early electrification and lightning [*Conway and Zrnić*, 1993; *Carey and Rutledge*, 1998]. *Woodard et al.* [2012] showed that the $+Z_{DR}$ columns are a useful parameter for radar-based operational forecasting algorithms for lightning initiation.

Many works have demonstrated that electric fields in clouds can also influence the orientation of ice crystals with oblate and prolate shapes [*Weinheimer and Few*, 1987; *Metcalf*, 1993, 1995; *Krehbiel et al.*, 1996; *Caylor and Chandrasekar*, 1996; *Metcalf*, 1997; *Foster and Hallett*, 2002; *Ventura et al.*, 2013; *Mattos et al.*, 2016]. In conditions of strong electric field ice crystals are mostly vertically oriented. When detected by polarimetric radars, these hydrometeors traditionally present negative values for differential propagation phase (Φ_{DP}) [*Caylor and Chandrasekar*, 1996; *Ryzhkov and Zrnic*, 2007; *Carey et al.*, 2009] and negative K_{DP} [*Caylor and Chandrasekar*, 1996; *Carey et al.*, 2009; *Hubbert et al.*, 2014a; *Mattos et al.*, 2016]. For example, *Caylor and Chandrasekar* [1996] found that Φ_{DP} and K_{DP} gradually decrease and then abruptly increase after lightning. The authors documented changes of 5° in Φ_{DP} and a systematic minimum peak in K_{DP} of approximately $-0.9° \, km^{-1}$ in the height range 7–14 km just before lightning occurrences. More recently, *Mattos et al.* [2016] documented the polarimetric behavior as a function of the lightning density and observed that negative K_{DP} is observable only in conditions with the strongest lightning frequency. However, the larger unaligned graupel-ice crystals mixture could mask the electrical alignment of ice crystals as indicated by the change in K_{DP} measurements as discussed in previous studies [*Marshall et al.*, 2009; *Carey et al.*, 2009]. *Carey et al.* [2009] evaluated the polarimetric signatures of ice particles using a T-matrix approach and found that in regions with $Z_H > 40$–$45 \, dBZ$, the $|K_{DP}|$ of graupel can be on the order of the $|K_{DP}|$ of vertically oriented plate ice crystals. These results suggested that in a graupel-plate mixture, horizontally oriented hydrometeors can mask the electrical alignment signature that would otherwise be present in the K_{DP} of vertically oriented plates alone. Recently, *Hubbert et al.* [2014a] evaluated the nature of the ice crystals causing negative K_{DP} in polarimetric measurements from S-band polarimetric radar. The results suggested two types of ice crystals: (1) smaller aligned ice crystals (columns or plates) with relatively small Z_H and (2) larger aggregates or graupel randomly oriented with larger Z_H that masks the Z_{DR} of the smaller aligned ice crystals. The interpretation of these results has been supported by satellite measurements. Satellite measurements at microwave frequencies (85 GHz) have shown negative differences in brightness temperature in the 85 GHz channel associated with strong lightning frequency [*Prigent et al.*, 2005; *Mattos and Machado*, 2011]. *Mattos and Machado* [2011] documented that CG lightning rate increases linearly with polarization reduction, suggesting that such polarization differences could be explained by relatively large and nonspherical particles that are mostly vertically oriented.

Some works showed also that stratiform regions of summer squall lines can exhibit strong electric fields sufficient for lightning initiation [*Chauzy et al.*, 1980; *Engholm et al.*, 1990], which could promote negative Z_{DR}. On the other hand, snowstorms with moderate snowfall rates probably do not have strong electric fields. For example, *Williams et al.* [2015] documented predominantly positive Z_{DR} in snowstorms and warm season stratiform systems, indicating that the vertical electric fields they contain are not sufficient to reorient ice crystals and change the sign of Z_{DR}.

Other works have documented that negative Z_{DR} could also be caused by graupel particles [*Wiens et al.*, 2005; *Dolan and Rutledge*, 2009; *Evaristo et al.*, 2013; *Homeyer and Kumjian*, 2015; *Stolzenburg et al.*, 2015; *Oue et al.*, 2015; *Bringi et al.*, 2016]. For example, *Dolan and Rutledge* [2009], using a T-matrix scattering model for several different hydrometeor types, suggested the presence of negative Z_{DR} associated with graupel particles. High-density graupel may have negative Z_{DR} values with relatively large reflectivity. Consistent with this picture, *Evaristo et al.* [2013] showed a linear decrease in Z_{DR} with the cone apex angle of conical graupel; for instance, a Z_{DR} of around $-1.2 \, dB$ was obtained for 30°. *Bringi et al.* [2016] documented negative Z_{DR} (from -0.3 to $-0.7 \, dB$) values along a vertical column in a winter storm in the high plains region of Colorado. The results suggested that conical graupel was more prevalent in the 3.5–4.0 km mean sea level (msl) height layer of the echo cores where Z_{DR} tended to be slightly more negative. *Homeyer and Kumjian* [2015] documented near-to-zero Z_{DR} minima in organized and discrete supercells close to and at altitudes higher than the updraft column features, indicating the presence of large hail. Additionally, minimum Z_{DR} and negative K_{DP} were observed throughout the portion of the convective cores of organized convective systems that overshot the tropopause, suggesting signatures from small hail and/or lump or conical graupel.

Understanding the relationships between the characteristics of polarimetric radar in the early development of clouds and the production of the first lightning could be very useful for lightning nowcasting and lightning parameterization. The basic aspects of cloud electrification have been described in several studies; however, cloud evolution during the electrification life cycle, from the first radar echo until the moment of the first IC and CG flashes, has not been completely defined. What is different for this work from prior studies is the

extensive documentation of the first IC and CG lightning flashes using two- and three-dimensional lightning location systems together with time-resolved polarimetric observations for a special subset of storms with lower attenuation. The thunderstorms studied in this work are very compact clouds (< 20 km diameter), and this procedure enabled a simpler physical interpretation of early thunderstorm development and with reduced radar attenuation operating at X-band. In addition, this study aims to evaluate the signatures from conical graupel using X-band polarimetric radar (XPOL) with signatures strongly tied to the initial electrification of these thunderstorms. Therefore, this study aims to cover these aspects based on case studies and a large statistical analysis of 46 isolated compact thunderstorm life cycles.

Section 2 presents the general aspects of the CHUVA-Vale campaign and the radar and lightning observations that were employed. Section 3 presents the methodology, section 4 discusses in detail three case studies, and section 5 provides the statistical analysis of the 46 thunderstorms. The discussion and the main conclusions are presented in section 6.

2. The CHUVA-Vale Campaign

The CHUVA (Cloud Processes of the Main Precipitation Systems in Brazil: A Contribution to Cloud Resolving Modeling and to the Global Precipitation Measurement) project's main scientific motivation was to contribute to the understanding of cloud processes, which represent one of the least understood components of the weather and climate system. For 5 years (from 2010 to 2014) the CHUVA project has conducted several field campaigns in Brazil (see *Machado et al.* [2014] for a detailed description). The CHUVA-Vale campaign's objective was to understand the cloud processes that evolve when clouds transform into thunderstorms. The CHUVA-Vale campaign took place during the Brazilian spring-summer (from November 2011 to March 2012) in São José dos Campos, in Southeast Brazil. The essential data sets used in this study were the polarimetric variables from the XPOL radar, the return stroke information provided by the Brazilian Lightning Detection Network (BrasilDAT), and the very high frequency (VHF) radiation sources from the São Paulo Lightning Mapping Array (SPLMA). Figure 1 shows the location of the XPOL radar (gray diamond) and the lightning sensors from the BrasilDAT (blue stars) and SPLMA (red filled circles) networks. Asterisks represent the locations of the 46 incipient thunderstorms at the time of the first CG lightning flash.

2.1. XPOL Radar and Data Postprocessing

To identify and track the polarimetric signatures in the thunderstorms, we utilized all the volume scans from the mobile XPOL (9.3 GHz) polarimetric radar. We evaluated the horizontal reflectivity (Z_H, dBZ), differential reflectivity (Z_{DR}, dB), specific differential phase (K_{DP}, °km^{-1}), and the correlation coefficient (ρ_{HV}) (see *Straka et al.* [2000] for a detailed description of these variables). The XPOL strategy was consistently performed every 6 min and included a 4 min standard volumetric scan with 13 elevations from 1.0° to 25.0° and radar samples resolved to 150 m in range and 1.0° in azimuth. The strategy also included a scan at 89° elevation with full azimuthal rotation for purposes of Z_{DR} calibration (offset check) and specific range-height indicator scans.

The radar data were postprocessed following several steps to correct the raw data for attenuation and the Z_{DR} offset. To correct the attenuation in Z_H, the so-called Rain Profiling Algorithm proposed by *Testud et al.* [2000] was applied. The reflectivity field was compared with the nearest S-band radar (50 km distant from XPOL radar). The XPOL radar captured very well the storm structure in comparison with the S-band radar. However, for higher XPOL reflectivity values (40–60 dBZ) a negative BIAS (around -5 dBZ) was found as well as for the comparison with the reflectivity simulated through the T-matrix method using information from the disdrometer. For higher reflectivity values the XPOL radar attenuation correction scheme does not fully correct the reflectivity field. Section 3 discusses this effect in the results and the limitations on the storm selection to reduce these uncertainties.

Differential attenuation in Z_{DR} is experienced when radiation moves through populations of oblate raindrops; this was corrected using the method of linear Φ_{DP}, which considers the total differential attenuation to be linearly proportional to Φ_{DP} [*Bringi et al.*, 2007]. The Z_{DR} average and median corrections were 0.3 and 0.2 dB, respectively. The offset in Z_{DR} due to the imbalance of the horizontal and vertical channels was determined for three periods of the CHUVA-Vale campaign: -0.27 dB (period before the exchange of the radome), -0.33 dB (period after the exchange of the radome), and -0.59 dB (period after the calibration/substitution of components) [*Sakuragi and Biscaro*, 2012].
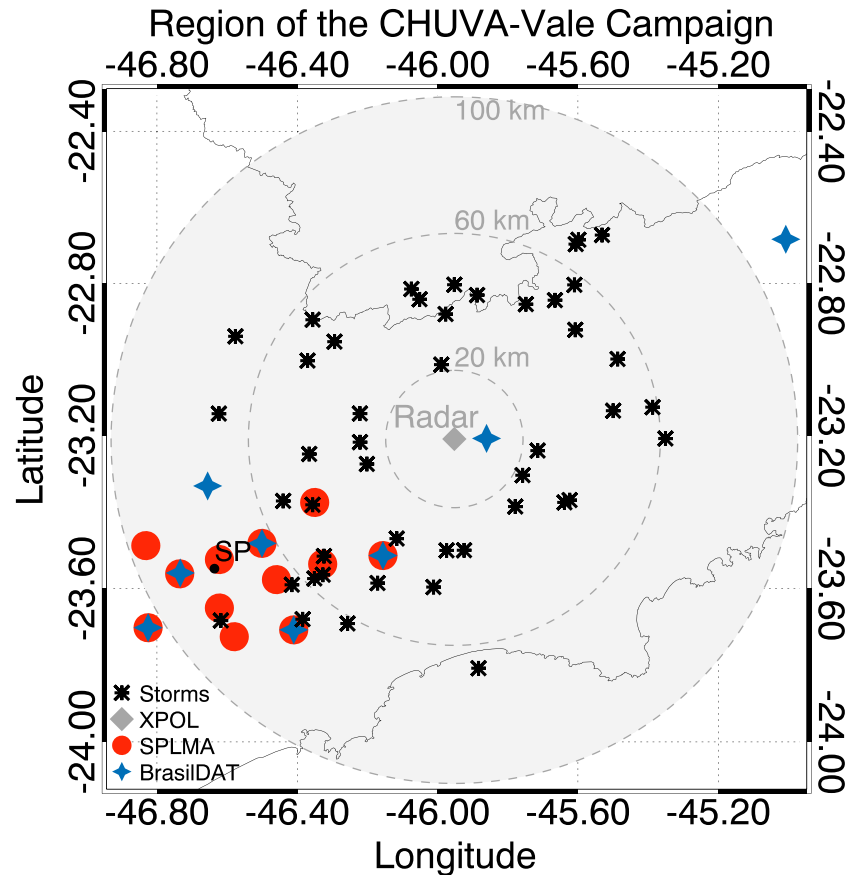
Figure 1. Region of the CHUVA-Vale campaign with the localization of the X-band radar (gray shaded region), and the SPLMA (red filled circles) and BrasilDAT (blue stars) lightning sensors. Asterisks represent the locations of the 46 thunderstorms at the time of the first cloud-to-ground (CG) lightning flash. The gray dashed lines represent the distance rings (20, 60, and 100 km) from the radar. The minimum detectable radar reflectivity at 20 km and 60 km range were -4 dBZ and 9 dBZ, respectively.

To compute K_{DP} an iterative finite impulse response range filter developed by *Hubbert and Bringi* [1995] was applied to the raw Φ_{DP} data. This filter smoothes Φ_{DP}, and an interactive methodology was performed to remove Φ_{DP} deviations caused by backscatter differential phase shift (δ) from large oblate particles. The K_{DP} values were derived by a least squares regression of Φ_{DP} over several range gates. The average δ observed for the data set was 0.3°. Comparisons between the polarimetric variables from the T-matrix method using a Joss disdrometer and the variables estimated by the XPOL radar showed average disagreements (radar-disdrometer) of -0.04 dB (Z_{DR}) and of -0.07 °km^{-1} (K_{DP}). Further details of the data postprocessing in the CHUVA experiment can be found in *Schneebeli et al.* [2012]. In the foregoing analysis, these corrections were included in the Z_H and Z_{DR} radar measurements.

2.2. Lightning Observations

Lightning information was provided by two independent Lightning Location Systems (LLSs). The IC and CG return strokes were provided by the Brazilian Lightning Detection Network (BrasilDAT) (Figure 1, blue stars). This lightning network employs technology from Earth Networks and operates over a large-frequency range (from 1 Hz to 12 MHz) and locates lightning using the time-of-arrival method. During this study, 56 sensors from BrasilDAT covered the southeastern, southern, central, and a portion of the northeastern regions of Brazil. Additional sensors from BrasilDAT were located close to the CHUVA-Vale region to improve the data quality. The reprocessed data pertaining to location, time of occurrence, and polarity of the IC and CG return strokes were used in this study. A preliminary evaluation of BrasilDAT using high-speed cameras showed a detection efficiency of about 88% for CG flashes [*Naccarato et al.*, 2012]. More recently, *Williams et al.* [2016] analyzed the same thunderstorms selected in this study and concluded that the majority of

lightning flashes detected by BrasilDAT was also detected by the Brazilian Integrated Lightning Detection Network (RINDAT) network. A good agreement was found between the CG stroke multiplicity and peak current estimated by BrasilDAT and RINDAT lightning networks. Additionally, a second LLS, operating in the VHF range, was used to determine the initiation region of the initial IC and CG return strokes detected by BrasilDAT. Named the São Paulo Lightning Mapping Array (SPLMA) (Figure 1, red filled circles), this network was developed by the New Mexico Institute of Mining and Technology and installed in a collaborative effort between the National Aeronautics and Space Administration, the University of Alabama in Huntsville, INPE (National Institute of Space Research), and USP (University of São Paulo). During the CHUVA-Vale campaign, the SPLMA was composed of 12 stations operating in the frequency band of TV channels 8 (180–186 MHz) and 10 (192–198 MHz) [*Blakeslee et al.*, 2013; *Bailey et al.*, 2014; *Albrecht et al.*, 2014]. The data set was reprocessed to provide the time, latitude, longitude, and altitude of the VHF radiation sources from all lightning detected during the campaign. The mean chi-square and mean number of stations per solution were 1.3 and 7, respectively. The SPLMA data were used for three thunderstorms for the analysis of lightning initiation (section 4). These thunderstorms occurred very close to the SPLMA center (less than 30 km distance), favoring a region with higher detection efficiency and enabling the detection of the majority of lightning activity from these thunderstorms.

3. Identification of Thunderstorms and Colocation With Lightning Observations

In this study, thunderstorms were identified and tracked manually with observations from the XPOL radar. These thunderstorms represent isolated precipitating cells and were chosen for further study if no additional thunderstorms were obstructing the path between the radar and the respective thunderstorm cell. This procedure enabled a simpler physical interpretation of early thunderstorm development and reduced radar attenuation effects characteristic of radars operating at X-band. A minimum distance of 20 km from the radar was selected to avoid thunderstorm cases with limited top due to the lower beam height close to the radar. Based on the aforementioned considerations, the life cycle of thunderstorms was typically sampled using a 6 min scan strategy, and the azimuth angle and distance limits from the radar were used to determine the thunderstorm's boundaries.

From the radar perspective, we considered thunderstorm initiation to be when a radar echo with any value of reflectivity above the reflectivity noise level was first detected in any height in any Plan Position Indicator (PPI) scan. The majority of thunderstorms were identified between 20 and 60 km range from radar, with minimum detectable radar reflectivity of approximately -4 dBZ and 9 dBZ, respectively. This procedure aimed to identify the initial development of the thunderstorms without restrictions. Based on these constraints, 46 thunderstorm life cycles were selected for this study.

The lightning information was colocated to each time step of the 46 thunderstorm life cycles. First, the return stroke observations from BrasilDAT were grouped into flashes using a temporal and spatial criterion of 0.5 s and 20 km, respectively. The 0.5 s time threshold is close to that employed by *McCaul et al.* [2009] and *Goodman et al.* [2005] (0.3 s) and *Nelson* [2002] (0.5 s). The criterion of 20 km corresponds to the fact that the majority of the 46 storms had diameters smaller than 20 km (see Figure 2 found in *Williams et al.* [2016]). *Williams et al.* [2016] used this same data set and spatial criterion and showed that the stroke multiplicity and peak current from BrasilDAT were very similar to values from the RINDAT network. In fact, the 20 km spatial criterion is a good choice for this study, because the storms are isolated and present low flash rates; however, for larger and more complex storms, other values for this spatial criterion should be evaluated. Afterward, IC and CG flashes were accumulated every 6 min and assigned to respective thunderstorms by using the area boundaries as a constraint. Finally, to determine the initiation height of these flashes, VHF sources from SPLMA were linked with the IC and CG flashes from BrasilDAT. The same spatial-temporal criteria used to combine strokes into flashes (i.e., 0.5 s and 20 km) were used to find the VHF sources associated with every IC and CG flash. In this way, a data set was created for the life cycle of each thunderstorm, from the polarimetric variables of the initial radar echo through the time of the first IC and CG flashes.

4. Thunderstorms Case Studies

In order to investigate the life cycle of the polarimetric variables and the microphysical properties of the regions where the first lightning initiates, we have analyzed on a case-by-case basis three thunderstorms

with different total (intracloud + cloud-to-ground) lightning flash rate: (i) relatively weak (1.5 flashes min^{-1}), (ii) relatively moderate (1.9 flashes min^{-1}), and (iii) relatively strong (2.3 flashes min^{-1}) lightning flash rate. These thunderstorms occurred close to the SPLMA center in a region with good coverage by the XPOL radar which made it possible to evaluate the region of initiation of the first flashes in terms of lightning and polarimetric radar signatures with good efficiency. Note that the designations of relatively weak, moderate, and strong lightning flash rate are based on the specific initial lightning flash rates for the small thunderstorms in this study, a procedure that differs from many other published studies. These thunderstorms present lower lightning flash rates likely due to their small size ($<$20 km diameter) and weaker updraft. Moreover, these definitions are used in this study as a reference and only to classify the lightning flash rates of these thunderstorms. In the context of the natural variability of the 46 selected thunderstorms, these three cases give a representative description of the studied thunderstorm population.

4.1. Case #1: The Thunderstorm at 1800 UTC on 20 February 2012

Time-height plots of selected radar parameters were computed for the thunderstorm life cycle based on the PPI-volume scans. For this purpose, the maximum Z_H in each PPI and the coincident value of Z_{DR}, K_{DP}, and ρ_{HV} in the cell were selected. Each volume scan of the thunderstorm was represented by a single vertical profile with 13 altitude levels, one for each PPI. Employing the methodology described above, the vertical sampling cannot be considered perfectly vertically aligned. However, a statistical evaluation of the degree of verticality of each profile showed a median value of 250 m offset between the vertical radar gates. This small effect is probably attributable to the compact and isolated thunderstorms that were selected in this study. This procedure aimed to illustrate the dominant behavior of the polarimetric parameters. Figure 2 shows the time-height plots of Z_H, Z_{DR}, K_{DP}, and ρ_{HV} from the first radar echo until the time of the first CG flashes for the thunderstorm with relatively weak total lightning flash rate (1.5 total flashes min^{-1}) observed on 20 February 2012.

The thunderstorm developed during late afternoon at 1800 UTC (1600 LT) and showed the first radar echo (at time of 0 min) at 3 km height and with 15 dBZ. The first IC (CG) flash was registered 28 (30) min after the first radar echo time. During this interval (from 0 to 30 min), the reflectivity Z_H (Figure 2a) evolves from weak (15 dBZ) to strong (56 dBZ) value at the 0°C level, indicating the formation of large hydrometers. For simplicity, the term "large hydrometers" is applied to those hydrometers that are in the Rayleigh regime ($<$2 mm diameter), hereafter. The time-height plot for Z_{DR} (Figure 2b) indicates an initial concentration of raindrops close to the melting layer which is shifted to higher altitudes when approaching the time of the first IC flash (at 28 min). At the time of the first CG flash (~30 min), a negative value of K_{DP} ($-0.3°$ km^{-1}, Figure 2c) and a strong value for ρ_{HV} ($>$0.99, Figure 2d) were found in upper levels (13 km altitude), suggesting that ice particles are being aligned by strong electric field. In fact, polarimetric variables show important characteristics between the 0° and -40°C levels. Figure 3 shows the evolution of the minimum values for Z_H, Z_{DR}, K_{DP}, and ρ_{HV} observed in the layer between 0° and -40°C. The reduction of Z_{DR} and K_{DP} before the first CG flash, followed by the increase of ρ_{HV} in the mixed layer (0° and -15°C), is the main remarkable behavior. It probably corresponds to the signature of the freezing of ice particles and the formation of graupel, fundamental conditions for the noninductive electrification mechanism and lightning production.

In order to evaluate the polarimetric behavior of the entire vertical structure of this thunderstorm, vertical cross sections were computed following the centroid of the thunderstorm (i.e., Lagrangian analysis) from the first radar echo until the time of the first CG flash. Figure 4 shows the vertical cross section as well as the projected locations of the flashes. The centroid location of the first 10% of the total sources in a flash was considered to be the origin location for the first IC and CG flashes, as in *Lang and Rutledge* [2008] and *Lund et al.* [2009]. The thunderstorm initiated with the formation of small raindrops with weaker Z_H (20 dBZ) in the warm cloud layer (Figure 4a) at 10 and 20 km range and after 6 min the supercooled raindrops reach the -16°C isotherm (Figure 4b) at 13 km range. The weaker Z_H (20 dBZ) and the moderate Z_{DR} (+1.5 dB) observed close to the -25°C level suggest the initial formation of ice crystals. After 6 min (Figure 4c) a well-defined +Z_{DR} column with strong Z_H (50 dBZ) and Z_{DR} (+3.5 dB) is observed close to the -15°C level at 13 km range. A drop freezing zone characterized by low ρ_{HV} (0.85) is identified at the top of the +Z_{DR} column, and ice crystals are predominant above this altitude. This minimum in ρ_{HV} at the top of the +Z_{DR} column is consistent with previous studies [*Bringi et al.*, 1997; *Hubbert et al.*, 1998; *Smith et al.*, 1999; *Kumjian et al.*, 2014; *Snyder et al.*, 2015] and suggests a region with a mixture of supercooled and partially frozen drops. Six minutes
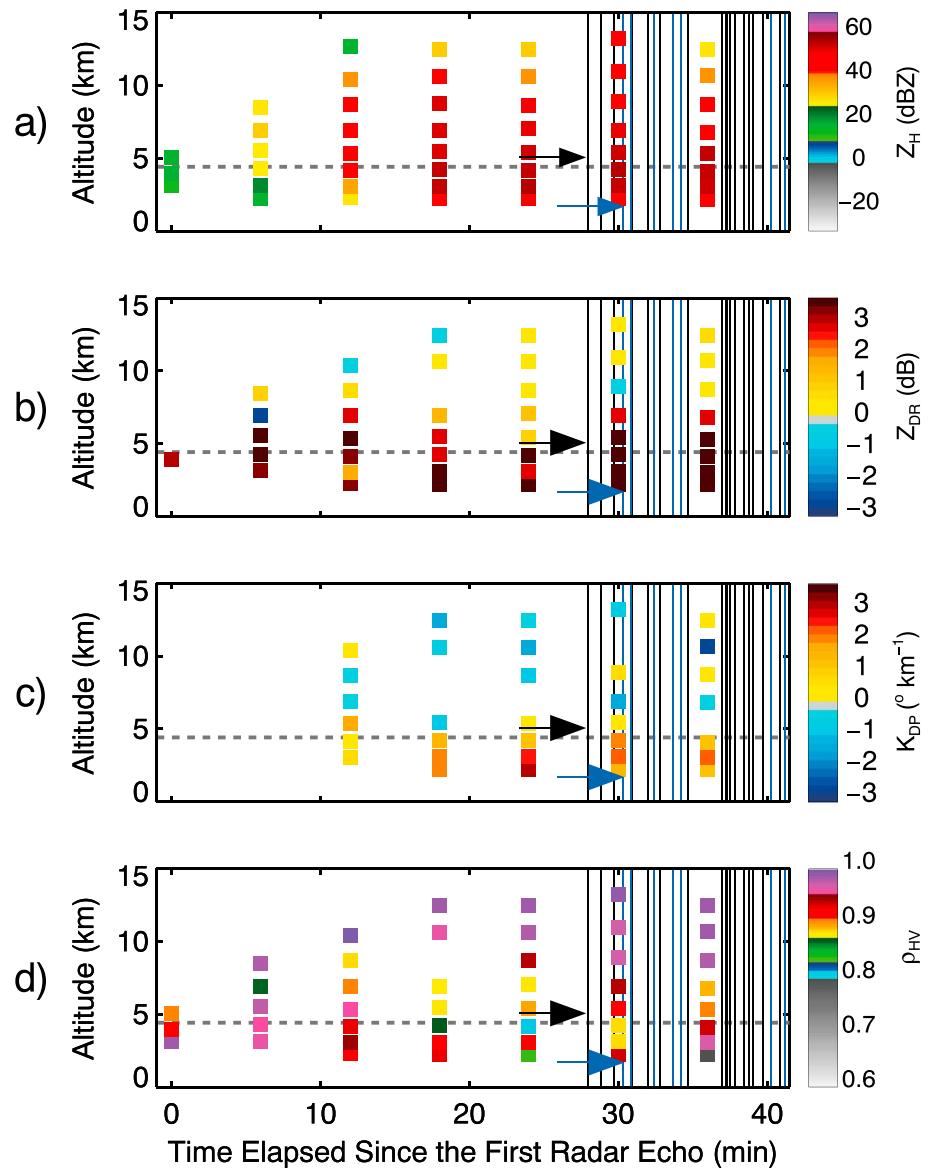
Figure 2. Time-height plot of (a) Z_H (dBZ), (b) Z_{DR} (dB), (c) K_{DP} (° km^{-1}), and (d) ρ_{HV} for the thunderstorm observed at 1800 UTC on 20 February 2012. The horizontal dashed line marks the 0°C level as determined by the sounding data. The black vertical lines in the figures represent the times of the intracloud lightning flashes, and the blue lines represent the cloud-to-ground lightning flashes. Arrows indicate the first intracloud (black) and the first cloud-to-ground (blue) flashes.

later (Figure 4d), this region intensifies and reaches higher levels and also reaches the ground, indicating the formation of large precipitation particles near the ground. Note the existence of a deepened tower reaching up to −16°C with strong Z_H and including a narrow tower of positive Z_{DR} above the melting layer, indicating the lofting of supercooled raindrops by strong updraft. Ice crystals and graupel particles are evident in the upper layers (>8 km) of this column, inferred by the negative Z_{DR} and K_{DP} in this region. In the following time step (Figure 4e) the Z_H value above the −30°C level centered at 13 km range decreases by 5–10 dBZ and a large region with more negative Z_{DR} and K_{DP} is formed simultaneously with the reduction of the +Z_{DR} column, promoting the occurrence of the first IC flash close to the −20°C level. The freezing of the supercooled raindrops aloft when the +Z_{DR} column is collapsing is the probable cause for the diminished Z_H, since the dielectric constant for ice is smaller than for liquid water particles [*Battan*, 1973]. The +Z_{DR} column collapse associated with the formation of graupel is evident in the image of the first CG flash (Figure 4f), where large conical graupel is suggested
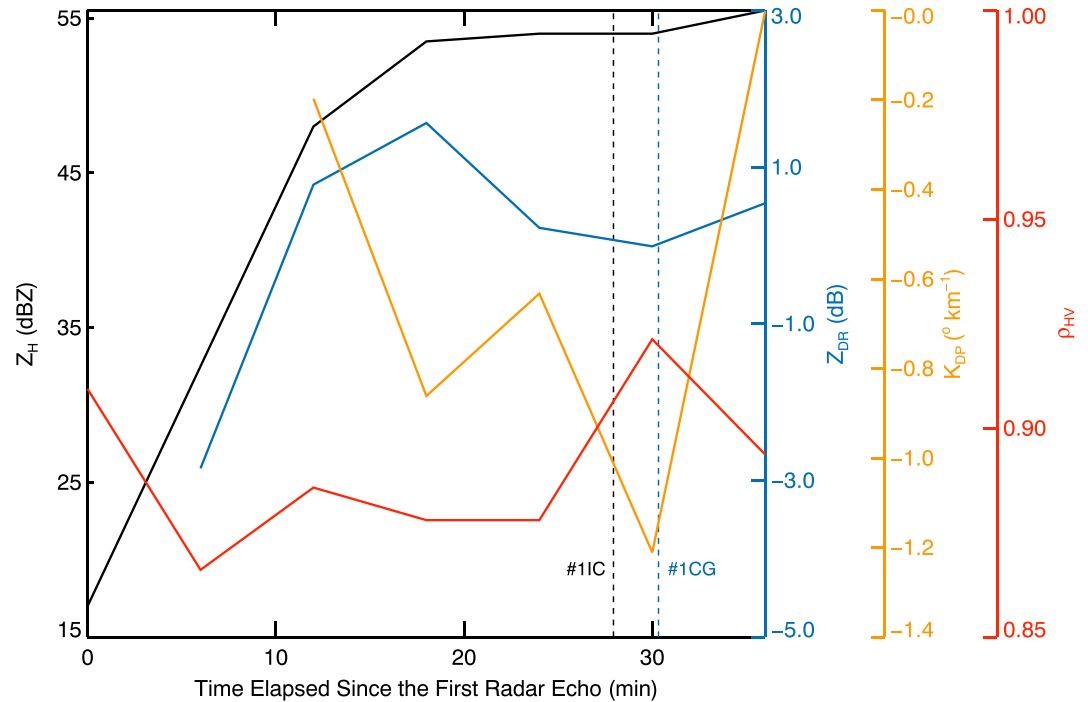
Figure 3. Maximum value of Z_H (dBZ) (black line) and minimum values of Z_{DR} (dB) (blue line), K_{DP} (° km^{-1}) (orange line), and ρ_{HV} (red line) in the cloud layer between 0° and -40°C for the thunderstorm evolution documented in Figure 2. The black and blue dashed lines mark the times of the first intracloud and cloud-to-ground flashes, respectively.

close to the melting level. In the follow image (Figure 4g), conical graupel particles are predominant above the melting layer when the IC flash rate increases.

4.2. Case #2: The Thunderstorm at 1536 UTC on 22 January 2012

The thunderstorm with relatively moderate total lightning flash rate (1.9 flashes min^{-1}) developed during the afternoon period at 1536 UTC (1336 LT), and 20 min after of the first radar echo (Figure 5), it registered its first IC flash (indicated by the black arrow). Three minutes after the first IC flash, the first CG flash was registered (indicated by the blue arrow). The first radar echo is observed at the 4.3 km altitude with weaker Z_H (Figure 5a, 15 dBZ), positive Z_{DR} (Figure 5b, +2 dB), and strong ρ_{HV} (Figure 5d, 0.96) suggesting initial raindrops. From the thunderstorm initiation time until the radar scan time (from 0 to 18 min) that marked the first IC and CG flashes, the radar observations show an increase in Z_H up to 51 dBZ, a decrease in Z_{DR} down to -0.1 dB and an increase in ρ_{HV} (0.99) at the 8 km altitude (-23°C level), suggesting the formation of graupel particles and ice crystals. Positives K_{DP} values (Figure 5c, +0.2° km^{-1}) at the 10 km altitude (~ -34°C) show the existence of large concentration of ice phase hydrometers. Note that around 12 min after the first radar echo a deep column of Z_{DR} (+2.7 dB) reached 6.5 km altitude (-13°C), suggesting a strong supply of supercooled raindrops before the first IC and CG flashes times. Similar to the previously discussed thunderstorm, this feature of supercooled liquid particles lofted by the thunderstorm's updraft in the mixed phase is now well recognized as a +Z_{DR} column [Hall et al., 1980; Caylor and Illingworth, 1987; Bringi et al., 1991; Conway and Zrnić, 1993; Ryzhkov et al., 1994; Hubbert et al., 1998; Smith et al., 1999; Kumjian et al., 2012, 2014; Snyder et al., 2015]. In fact, these changes are more conspicuous in the mixed layer (between 0° and -15°C). Figure 6 shows an increase of K_{DP} (up to +0.4° km^{-1}), while Z_{DR} decreases (down to 0 dB) prior to the IC flash time.

It is noted that the convective process was initiated by two adjacent +Z_{DR} columns (Figure 7b, 1542 UTC) localized at ranges of 6 km and 11 km, likely associated with two convective updraft regions. In this distance range (6 km and 11 km) very small pockets of low ρ_{HV} (0.85–0.90) are observed at the top of the +Z_{DR} columns. These observations are qualitatively consistent with previous studies [Herzegh and Jameson, 1992; Conway and Zrnić, 1993; Jameson et al., 1996; Bringi et al., 1997; Hubbert et al., 1998] and are likely regions containing a mixed phase with supercooled drops, partially freezing drops and frozen
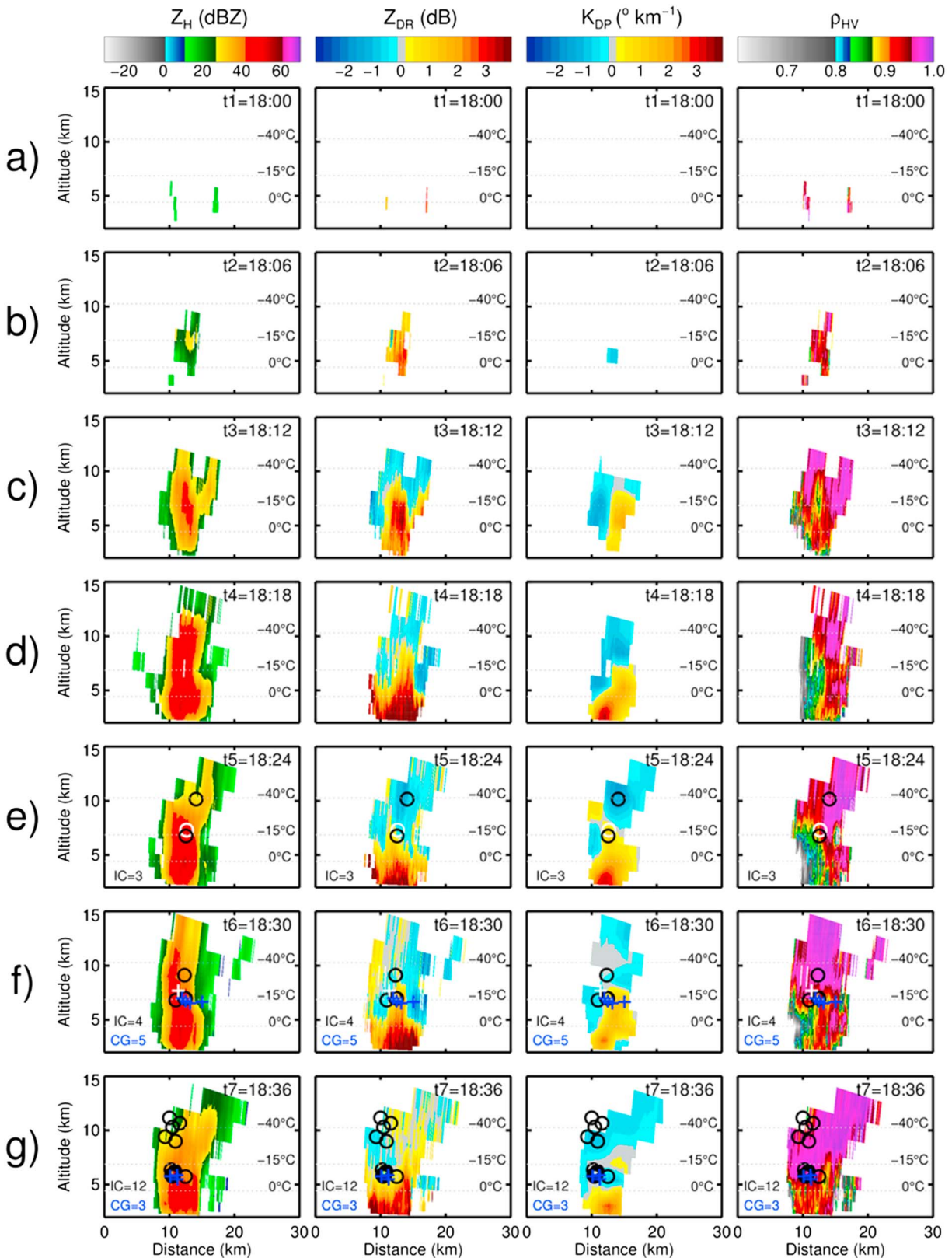
Figure 4. (a–g) Vertical cross sections of the polarimetric variables (Z_H, Z_{DR}, K_{DP}, and ρ_{HV}) for the thunderstorm evolution documented in Figure 2. The locations of the initiation points for the intracloud flashes are indicated with black circles and for the cloud-to-ground flashes by blue crosses. Symbols in white indicate the first intracloud (circle, Figure 4e) and cloud-to-ground flashes (cross, Figure 4f).
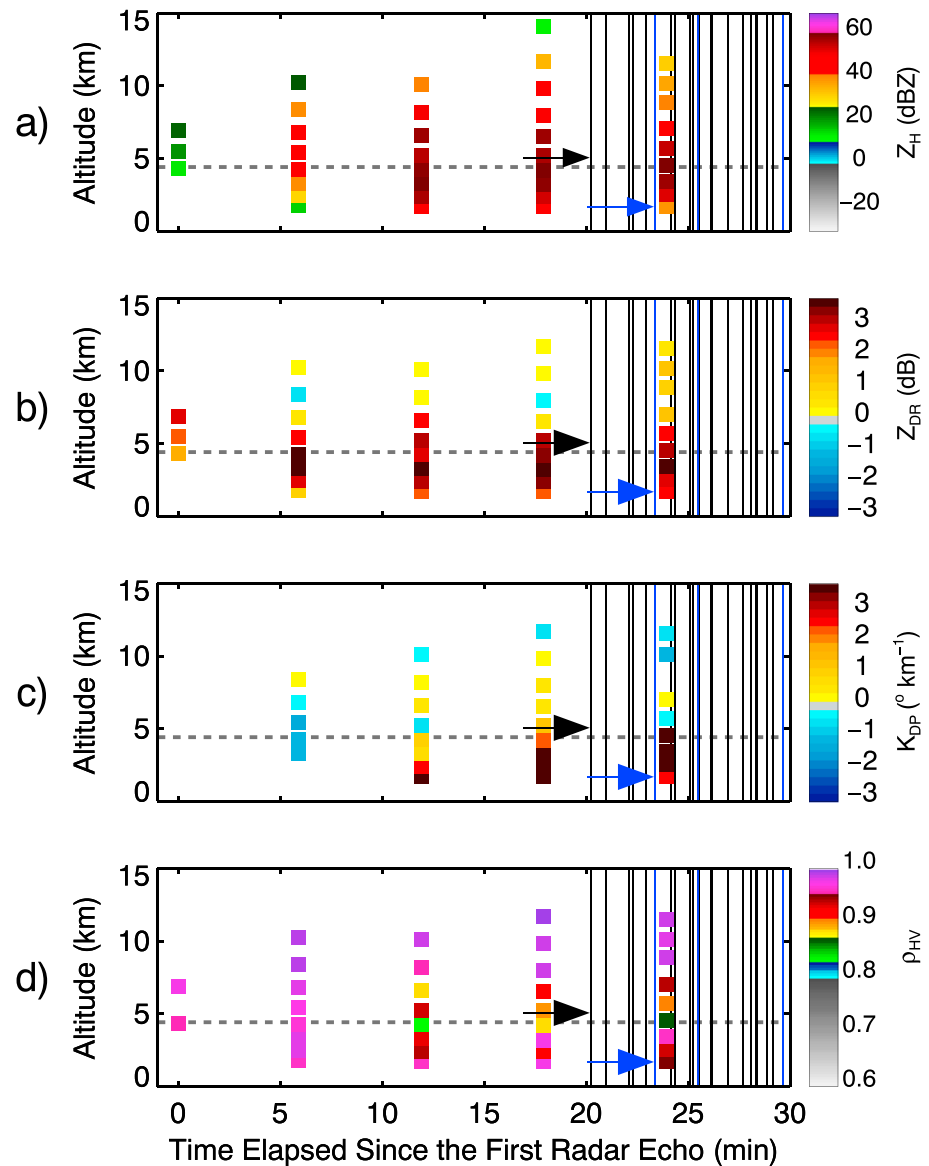
Figure 5. Time-height plot of (a) Z_H (dBZ), (b) Z_{DR} (dB), (c) K_{DP} (° km^{-1}), and (d) ρ_{HV} for the thunderstorm observed at 1536 UTC on 22 January 2012. The horizontal dashed line marks the 0°C level as determined by the sounding data. The black vertical lines in the figures represent the times of the intracloud lightning flashes, and the blue lines represent the cloud-to-ground lightning flashes. Arrows indicate the first intracloud (black) and the first cloud-to-ground (blue) flashes.

hydrometeors. The two $+Z_{DR}$ columns merged into a single column and descended close to the -10°C isotherm at 10 km range and negative K_{DP} ($-0.5°$ km^{-1}) was observed between 0° and -15°C, suggesting the formation of graupel particles (Figure 7c, at 1548 UTC). This demise of the $+Z_{DR}$ column produced mixed-phase hydrometeors such as graupel and supercooled raindrops as indicated by the low ρ_{HV} (0.85) at the 12 km range observed between the 0° and -15°C level. In the following moments (Figure 7d, at 1554 UTC) a large heterogeneous horizontal distribution of hydrometeors was observed from 5 to 17 km range and more pronounced between the 0°C and -15°C levels and the first IC was recorded (white circle); 3 min later (as described in Figure 5), the first CG flash (white cross) was recorded. The first IC flash initiated near the -30°C level at 8 km range, close to a region with vertically oriented ice crystals, and the first CG flash were recorded over the region close to the -3°C level at 13 km range, with strong reflectivity at the top of region with near-to-zero Z_{DR} with positive K_{DP} ($\sim+0.5°$ km^{-1}) and in a transition region with moderate to strong ρ_{HV} (~0.86–0.95), separated by a region with large negative Z_{DR}, which was likely
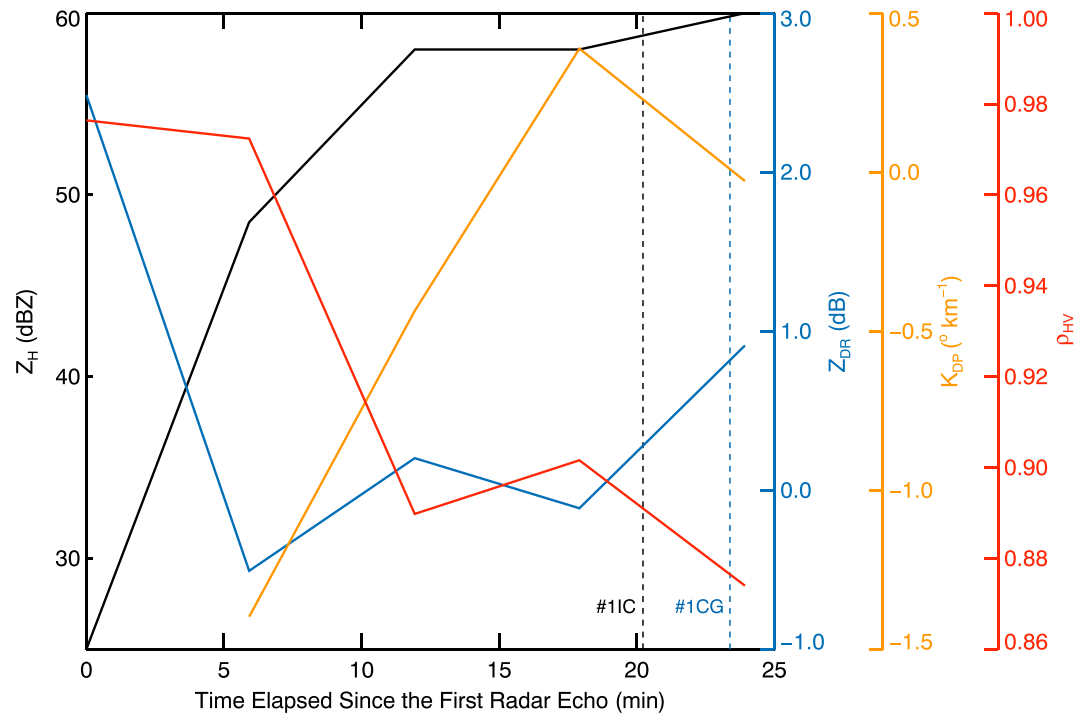
Figure 6. Maximum value of Z_H (dBZ) (black line) and minimum values of Z_{DR} (dB) (blue line), K_{DP} (° km^{-1}) (orange line), and ρ_{HV} (red line) in the cloud layer between 0° and −40°C for the thunderstorm evolution documented in Figure 5. The black and blue dashed lines mark the times of the first intracloud and cloud-to-ground flashes, respectively.

dominated by rimed graupel. The notable region with very low very ρ_{HV} (~0.80) between the 0°C and −15°C levels centered at 11 km range is likely associated with nonuniform beam filling (NBF) effects. According to *Ryzhkov* [2007], large cross-beam gradients of Φ_{DP} may cause a noticeable decrease of ρ_{HV}. *Ryzhkov* [2007] documented a negative bias of approximately 0.2 in ρHV. Although this bias exists, correcting ρ_{HV} for such bias is not practical because the bias cannot be estimated with sufficient accuracy.

4.3. Case #3: The Thunderstorm at 1818 UTC on 7 February 2012

Figure 8 shows the time-height plots for the thunderstorm that showed a relatively strong total lightning flash rate (2.5 flashes min^{-1}) observed on 7 February 2012. This thunderstorm developed during the late afternoon at 1818 UTC (1618 LT) and produced its first IC (CG) flash 31 min (38 min) after the initial radar echo. Actually, one can note a rapid intensification of the thunderstorm between 9 and 20 min after the initial radar echo with strong reflectivity (46 dBZ) and moderate Z_{DR} (+2.3 dB) reaching up to the 8 km altitude (−23°C level). The formation of the initial ice phase hydrometers is indicated by the appearance of the negative Z_{DR} (−0.1 dB) at 20 min close to the cloud top (10 km altitude, −38°C). At the moment of the first IC flash (~29–31 min), positive Z_{DR} (+3.5 dB) and K_{DP} (+3° km^{-1}) were observed close to 7 km altitude (−16°C), suggesting a rapid increase in the concentration of supercooled raindrops, which have contributed to the initial formation of the ice crystals and graupel in this layer. The ice crystal formation occurs through activation of ice nuclei within the updraft or associated with ice multiplication processes. The Hallet-Mossop mechanism [*Hallett and Mossop*, 1974] is largely accepted as a dominant ice multiplication process and occurs as small ice splinter from graupel growing by riming of supercooled droplets in the temperature range between −3° and −8°C.

After that time, and leading up to the time of the first CG flash (at approximately 35 min), the IC flash rate increased. At 37 min a column of negative K_{DP} (Figure 8c, minimum of −1.0° km^{-1} at 6 km altitude, ~−9°C) was observed in the altitude range between 6 and 14 km (between −9° and −64°C), while the ρ_{HV} value (Figure 8d) close to 10 km altitude decreased dramatically from 0.97 to 0.83, between the time of the first IC flash (at 30 min) and the time of the first CG flash (at 35 min), indicating the freezing of hydrometers and a mixture with supercooled raindrops. In fact, in the mixed layer, Z_{DR} and K_{DP} reached their minimum
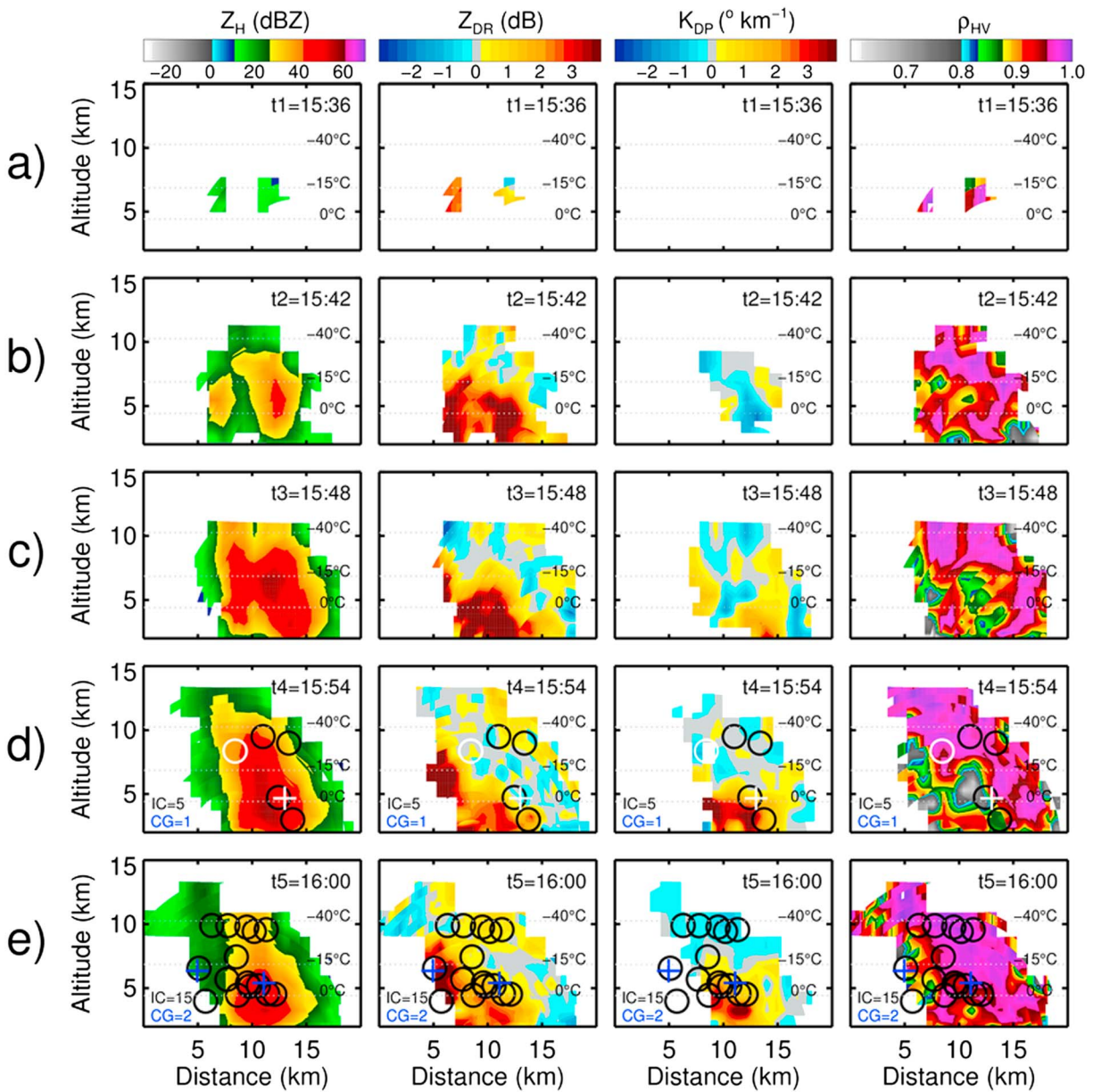
Figure 7. (a–e) Vertical cross sections of the polarimetric variables (Z_H, Z_{DR}, K_{DP}, and ρ_{HV}) for the thunderstorm evolution documented in Figure 5. The locations of the initiation points for the intracloud flashes are indicated with black circles and for the cloud-to-ground by blue crosses. In Figure 7d the symbols in white indicate the first intracloud (circle) and cloud-to-ground (cross) flashes.

values ($+0.2\,dB$ and $-1.1°\,km^{-1}$) and strong reflectivity ($>55\,dBZ$) prior to the CG flash time (Figure 9), probably associated with signatures from conical graupel.

The aforementioned observations are more evident in the vertical cross sections (Figure 10). We can note a slow increase in Z_H in the thunderstorm during the first 13 min (Figures 10a–10d) before the convection became intense. Two convective towers with large Z_H and Z_{DR} indicating strong updrafts were observed at ranges of 12 km and 17 km, respectively, and were extending up to approximately $-15°C$ (Figure 10e). At 1843 UTC (Figure 10f), these convective towers began to merge, and a deep and narrow column with positive Z_{DR} ($+3.5\,dB$) and moderate ρ_{HV} (~0.95) in the 14 km range formed, demonstrating the lofting of supercooled raindrops by strong updrafts. In addition, low ρ_{HV} (~0.85) indicating a freezing zone, as a result of the mixture of ice and liquid particles, is observed at the top of a secondary Z_{DR} column close to the $-15°C$ isotherm at 17 km range. In fact, after 4 min of this observation, the first IC flash was recorded (1847 UTC, Figure 10g). This
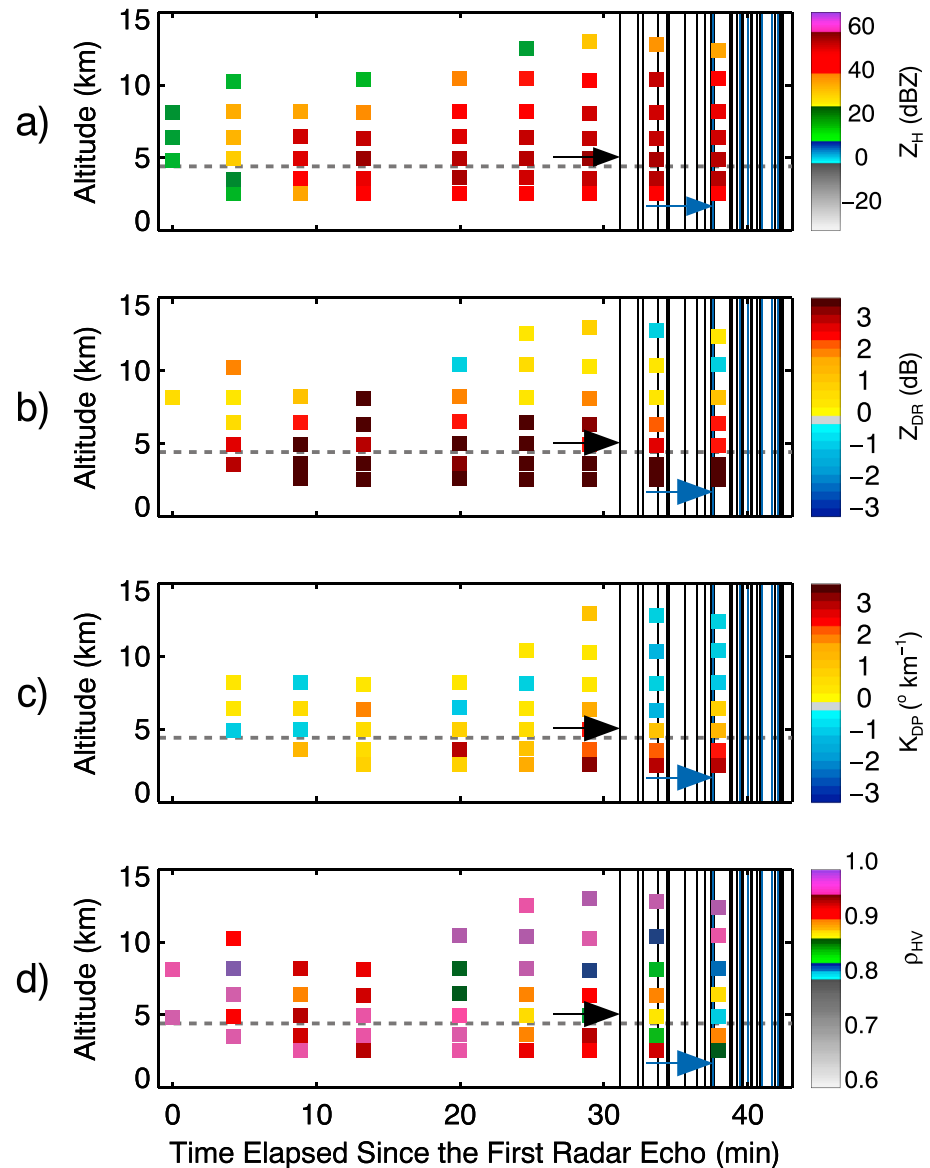
Figure 8. Time-height plot of (a) Z_H (dBZ), (b) Z_{DR} (dB), (c) K_{DP} (° km^{-1}), and (d) ρ_{HV} for the thunderstorm observed at 1818 UTC on 7 February 2012. The horizontal dashed line marks the 0°C level as determined by the sounding data. The black vertical lines in the figures represent the times of the intracloud lightning flashes, and the blue lines represent the cloud-to-ground lightning flashes. Arrows indicate the first intracloud (black) and the first cloud-to-ground (blue) flashes.

flash initiated close to the −10°C isotherm at the time when the +Z_{DR} column decreased and the cells with strong Z_H completely merged. A mixture of frozen drops, graupel, and ice particles is inferred in this region with low ρ_{HV} (~0.85) and negative/positive K_{DP} (between −0.5 and +0.5° km^{-1}) in the 10–17 km range between the −10° and −30°C levels and indicates that these hydrometers likely contributed to noninductive charging of ice hydrometeors and the formation of the first lightning flashes.

These regions with strong updrafts are inferred indirectly from observations of +Z_{DR} columns with strong Z_H. At the time of the first CG flash, at 1852 UTC (Figure 10h), negative K_{DP} (down to −0.5° km^{-1}), weaker-to-moderate Z_{DR} (down to −0.5 dB), and a large region with weaker ρ_{HV} (down to 0.85) are predominant signatures down to the −15°C level at 15 km range, suggesting the freezing of supercooled raindrops and the existence conical graupel. Probably, the graupel grows to a size too large to be sustained by updrafts and then begin to fall and ultimately melt, promoting the formation of large raindrops close to the surface. Although the initiation regions of both IC and CG flashes show evidence for
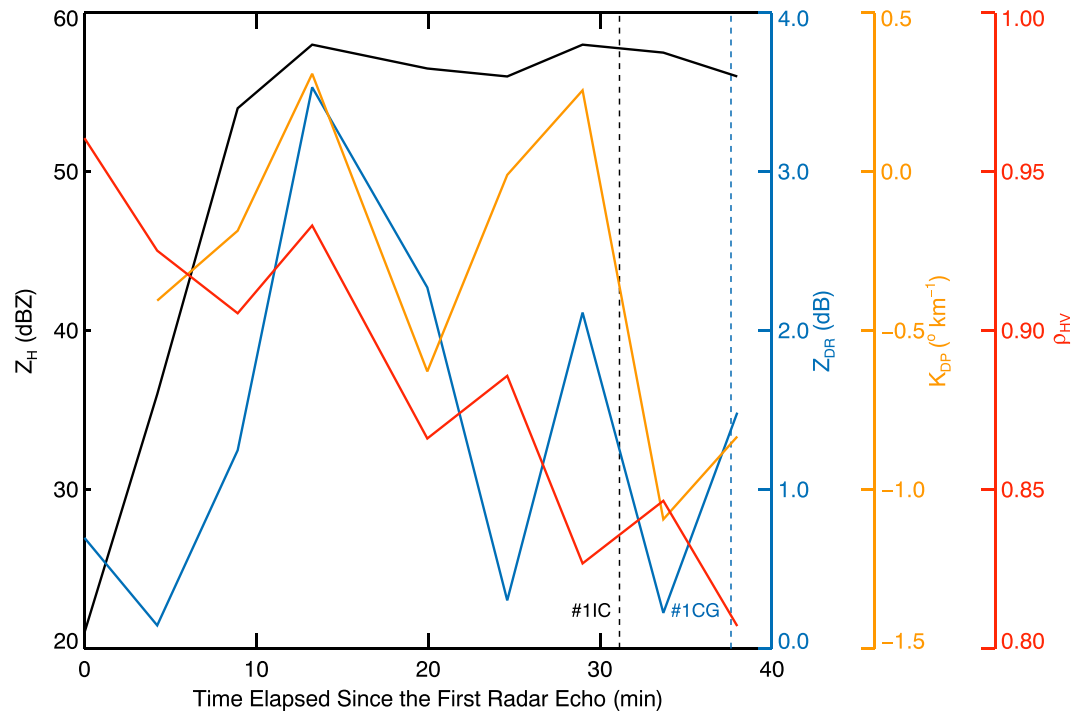
Figure 9. Maximum value of Z_H (dBZ) (black line) and minimum values of Z_{DR} (dB) (blue line), K_{DP} (° km^{-1}) (orange line), and ρ_{HV} (red line) in the cloud layer between 0° and −40°C for the thunderstorm evolution documented in Figure 8. The black and blue dashed lines mark the times of the first intracloud and cloud-to-ground flashes, respectively.

similar microphysical conditions, one could suggest that a large region with strong negative Z_{DR} and K_{DP} in the altitude range above the −15°C isotherm is a predominant signature at the time of the first CG flash.

Although the last two cases showed distinct and separate double reflectivity maxima (which indicated the existence of two distinct updraft maxima), the merging of two updrafts columns in this case seems not a physical requirement for lightning occurrence. The majority (80% of 46 cases) of the thunderstorms in this study showed only one reflectivity maximum (not shown). These results are consistent with *Goodman et al.* [1988] that documented the first IC flash after the hail was initially indicated by radar, during a period of rapid vertical development as the cloud top neared its maximum height and the first CG flash occurred when the maximum reflectivity core descended. Instead, the pronounced positive Z_{DR} in the layer between 0° and −15°C, followed by a decrease of the Z_{DR} in this region, is the most consistent characteristic of the storm evolution to lightning occurrence documented in this study.

5. Statistical Evaluation of the 46 Thunderstorms

This section presents the general behavior of the 46 thunderstorm life cycles selected in this study. Initially, the time lag between the first IC and the first CG flashes (Figure 11a) and the time lag between the first radar echo and the occurrence of the first IC and CG flashes (Figure 11b) were computed. For the large majority (98%) of thunderstorms, an IC flash preceded the first CG flash. Note that the mean time difference between IC and CG flashes was approximately 6 min and the median time difference was about 4 min. Only one thunderstorm exhibited a CG flash as its first flash. This overall behavior bears a close similarity to the earlier results (considering the mean values), particularly *Workman and Reynolds* [1949] (6 min), *Goodman et al.* [1988] (5 min), *Williams et al.* [1989] (6 min), *Harris et al.* [2010] (4.7–6.9 min), *Seroka et al.* [2012] (2.4 min), and *Stolzenburg et al.* [2015] (4.6 min). These results suggest that the predominance of the IC lightning in early stages is likely due to the vertical velocity and growth of ice particles and radar reflectivity above the negatively charged center. On the other hand, the occurrence of CG lightning has been documented in previous studies close to regions with graupel and hail descending below the negative charge center [*Goodman et al.*, 1988; *Carey and Rutledge*, 1996; *López and Aubagnac*, 1997; *Tessendorf et al.*, 2007]. The three case
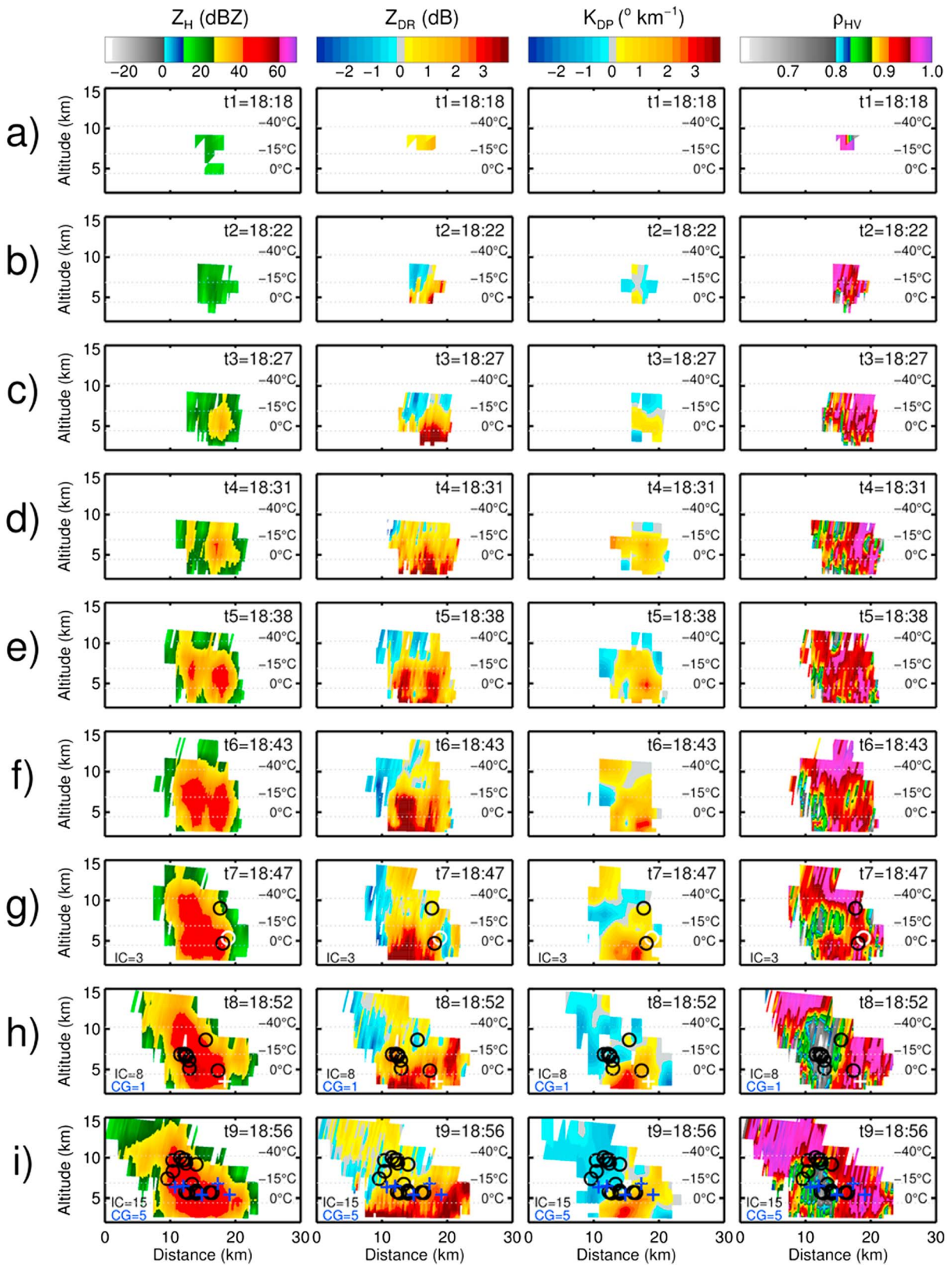
Figure 10. (a–i) Vertical cross sections of the polarimetric variables (Z_H, Z_{DR}, K_{DP}, and ρ_{HV}) for the thunderstorm evolution documented in Figure 8. The locations of the initiation points for the intracloud flashes are indicated with black circles and for the cloud-to-ground by blue crosses. Symbols in white indicate the first intracloud (circle, Figure 10g) and cloud-to-ground flashes (cross, Figure 10h).
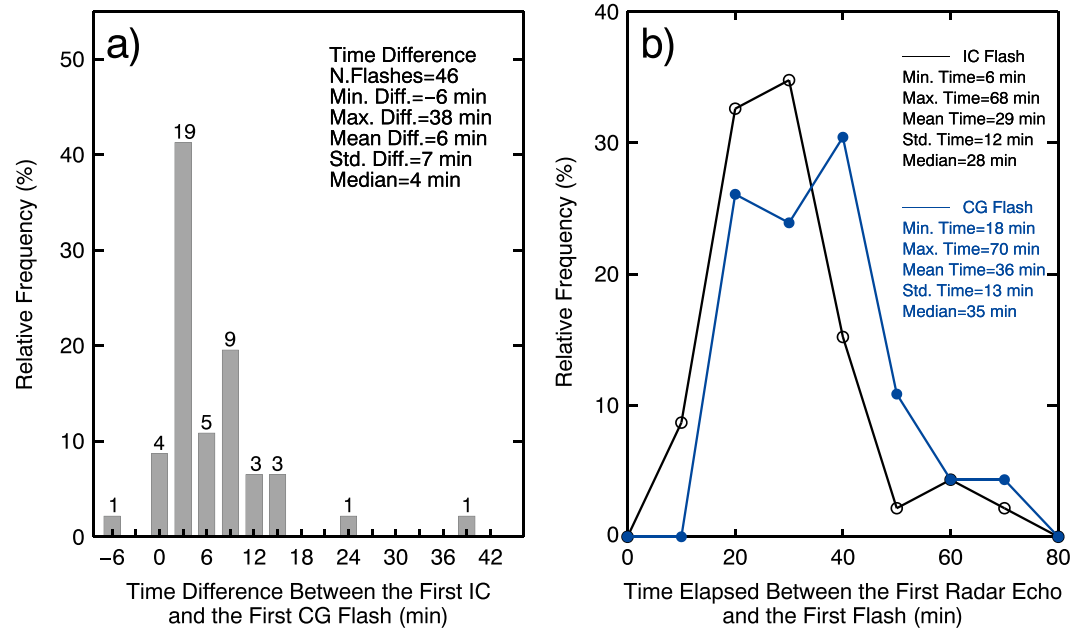
Figure 11. Relative frequency distribution of the (a) time difference in minutes between the first intracloud (IC) and the first cloud-to-ground (CG) lightning flash and (b) elapsed time between the first radar echo and the first intracloud (black line) and the first cloud-to-ground (blue line) lightning flash for the 46 thunderstorms.

studies previously presented (i.e., Figures 4, 7, and 10) corroborate these findings, showing the first IC preceding the first CG flash at the boundary of the negative Z_{DR} layer. Figure 11b shows IC flashes occurring, on average, approximately 29 min after the initial radar echo, while CG flashes were most frequently delayed by approximately 36 min. Only for few thunderstorms, the first flash occurs as much as 50 min later, or more. Studies using satellite only [*Harris et al.*, 2010] or a combination of satellite and radar [*Mecikalski et al.*, 2013] have documented a time elapsed for the lightning initiation on the order of 30–60 min. Since sensors on geostationary satellites detect clouds rather than precipitation, larger time differences are expected in comparison to those values documented in our study. Other studies employing radar reflectivity values at various heights have documented lead times for lightning initiation of about 10–20 min [*Dye et al.*, 1989; *Buechler and Goodman*, 1990; *Hondl and Eilts*, 1994; *Gremillion and Orville*, 1999; *Vincent et al.*, 2004; *Yang and King*, 2010; *Mosier et al.*, 2011]. The time elapsed to the lightning initiation depends on the criterion used to define the first radar echo or cloud initiation and the environmental instability conditions. In our case we have considered as the first radar echo any reflectivity value (any value above the local noise floor of the radar) at any height. The detection of this earlier first echo could be responsible for the long time observed. In addition, the thunderstorms selected from the CHUVA-Vale campaign were small, compact and isolated and grew in an environmental with low-to-moderate Convective Available Potential Energy (CAPE) and low wind shear, indicating a slow growth of precipitating cells and hydrometers. Consistent with this approach, *Mecikalski et al.* [2013] have compared two groups of storms, with smaller (1458 J kg^{-1}) and greater (2512 J kg^{-1}) CAPE and found that the smaller CAPE storms are characterized by slower and steadier or development rates. The storms with lower CAPE likely possess weaker updrafts and display earlier development of warm rain processes. We believe that, when an organized mesoscale system is considered, we should expect a shorter time. This supports the idea on the existence of the slower thunderstorm development associated with an early warm rain phase in the developing cloud. As a consequence of this slow process, the graupel and ice crystals in the mixed layer take a longer time to grow and activate the lightning initiation. Moderate CAPE supports the likely occurrence of moderate updrafts in these small thunderstorms, leading to a moderate in-cloud charging process. In fact, for the great majority (85%) of thunderstorms, the first echoes are warm rain echoes (Figure 12a) with mean height around 2 km and with weaker Z_H (25 dBZ) related to moderate Z_{DR} (up to +4 dB) (Figure 12b). These observations are consistent with the results presented by *Tuttle et al.* [1989] that
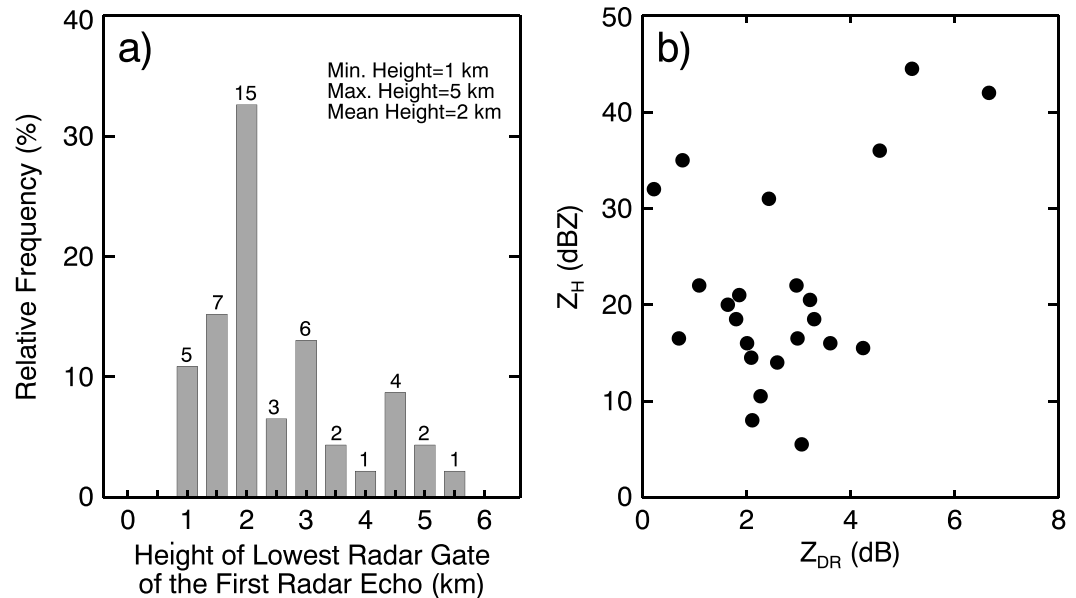
Figure 12. (a) Relative frequency distribution of the height (km) of lowest radar gate at time of the first radar echo and (b) scatterplots between Z_H (dBZ) and Z_{DR} (dB) for the lowest radar gate at time of the first radar echo.

documented the storm's first echo below the melting level, suggesting precipitation development was through warm rain processes (e.g., accretion and coalescence growth). Our results suggest that the air in which the thunderstorms are growing is relatively moist and clean, or the ascent speed close to the cloud base height is on the low side (to enable more time for warm rain coalescence).

In order to evaluate the statistical distribution of the polarimetric variables, whisker plots were compiled for all thunderstorms, for each cloud's altitude range at different life cycle times. The thunderstorm life cycle was studied at four specific times: (i) the time of the first radar echo, (ii) the intermediate time between the first radar echo and the first IC flash, (iii) the time of the first IC flash, and (iv) the time of the first CG flash. Hereafter, the analysis will focus on these four times, which are named as follows: #1Echo, Int., #1IC, and #1CG. Consistent with the procedure followed by *Mattos et al.* [2016], radar vertical profiles of the thunderstorm can be separated into four altitude layers: (i) warm (below 0°C), (ii) mixed 1 (from 0° to −15°C), (iii) mixed 2 (−15° to −40°C), and (iv) glaciated phase (from −40° to −65°C). These layers were chosen due to the different physical behaviors related to the thunderstorm electrification process observed by *Mattos et al.* [2016]. Figure 13 presents the whisker plots for all four thunderstorm layers in the four different lifetimes.

Generally, the initial radar echo in the warm layer of thunderstorms shows Z_H greater than 10 dBZ, suggesting the cloud growth associated with initial updrafts in the life cycle stages (Figure 13a, red boxes, #1Echo). We should remember that the maximum Z_H value was chosen by PPI in this study, and this certainly influences the higher Z_H values found in the analysis. We note that Z_H in the warm layer (Figure 13a, red boxes) exhibits the major differences among the polarimetric variables over the thunderstorm life cycle (from #1Echo to #1CG). This result indicates that hydrometeors with different sizes can be inferred prior to the first CG flash. Note that ρ_{HV} (Figure 13d, red boxes) in the warm layer shows a certain variability; it is larger at the time of the first radar echo, probably associated with the large differences in droplet sizes and then decreases slightly as the thunderstorm evolves to the first CG flash. Although very large raindrops (>2 mm in diameter) represent only a small percentage (<4%) of the raindrops observed in the warm layer for this study (not shown), resonance effects and non-Rayleigh regime produced by these raindrops could be contributing to the strong positive Z_{DR} (above +5 dB) and low ρ_{hv} (below 0.90) values observed in the warm layer [*Ryzhkov and Zrnic*, 2005].

The distribution of K_{DP} (Figure 13c, red boxes) presents a spreading leading to the time of the first CG flash in the warm layer, suggesting the formation of a strong concentration of flattened raindrops. Since K_{DP} is
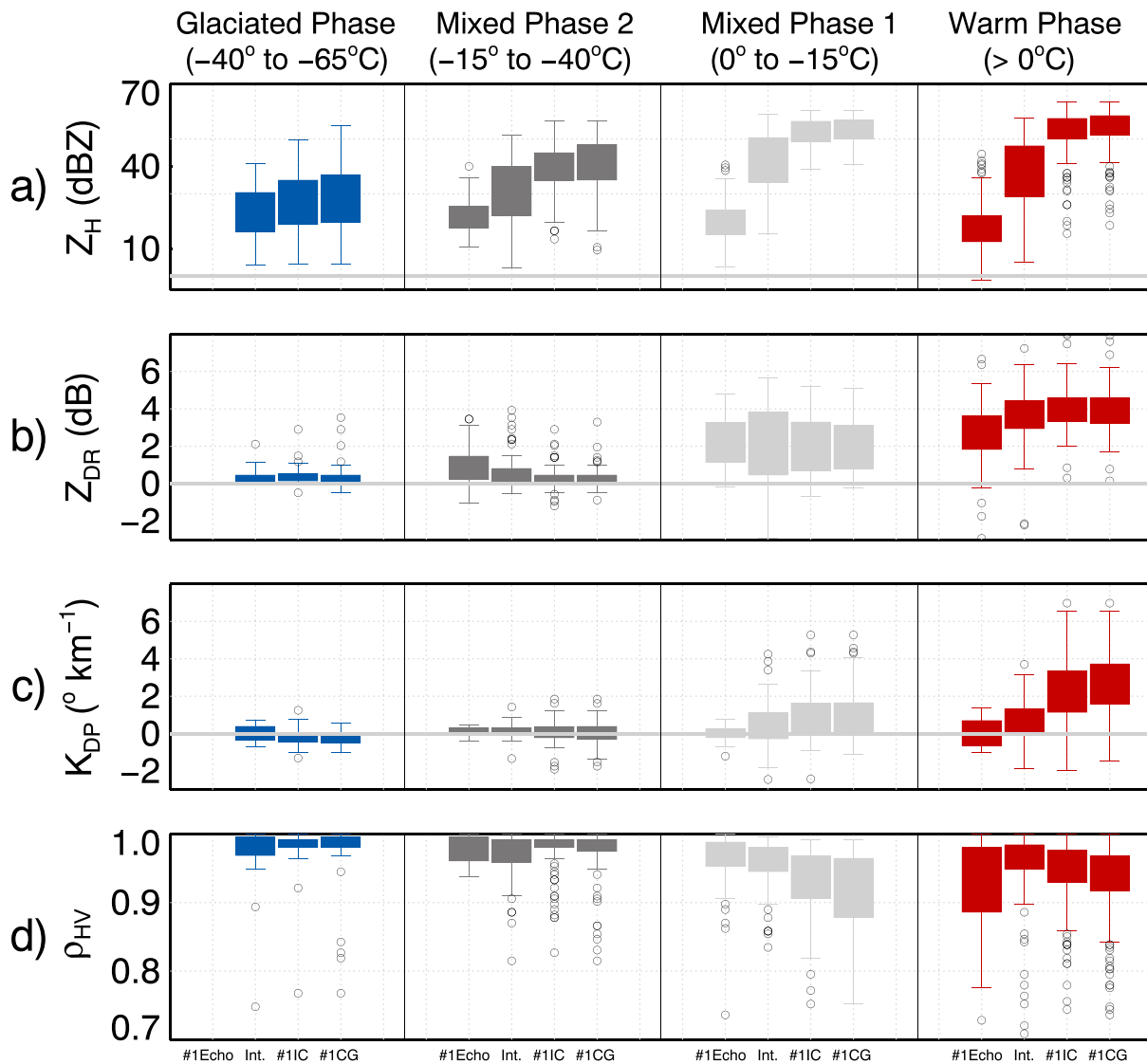
Figure 13. Box and whiskers plots for (a) Z_H (dBZ), (b) Z_{DR} (dB), (c) K_{DP} (° km^{-1}), and (d) ρ_{HV} for the glaciated (from −40° to −65°C, blue boxes), mixed 2 (−15° to −40°C, dark gray boxes), mixed 1 (from 0° to −15°C, light gray boxes), and warm (below 0°C, red boxes) phase layers. For every layer, the four boxes represent the following stages of the thunderstorm life cycle: (i) the time of the first radar echo (#1Echo), (ii) the intermediate time between the first echo radar and the first intracloud lightning flash (Int.), (iii) the time of the first intracloud lightning flash (#1IC), and (iv) the time of the first cloud-to-ground lightning flash (#1CG).

dependent on raindrop concentration [*Straka et al.*, 2000] and several studies have shown a good relationship between K_{DP} and rain estimates [*Zrnić and Ryzhkov*, 1996; *Ryzhkov et al.*, 2005], one can infer that the rain rate likely is increasing from the time of the first radar echo to the first CG flash. However, it is possible that in part, the dispersion observed in K_{DP} in the warm layer is linked to nonuniform beam filling effects (NBF) [*Gosset*, 2004; *Ryzhkov and Zrnic*, 2005]. It is important to note that comparisons between the polarimetric variables from the T-matrix method using a Joss disdrometer and the variables estimated by the XPOL radar showed a median disagreement (radar-disdrometer) in K_{DP} of −0.07° km^{-1}, indicating that NBF effects likely has reduced impact in this study.

The K_{DP} distribution at the time of the first IC and CG flashes in the mixed 1 layer (Figure 13c, light gray boxes) was similar; i.e., both distributions show large positive K_{DP} (up to +1.5° km^{-1}). A large variability in the intermediate time in this layer was also noted. This is possibly related to the +Z_{DR} column, which is better defined at the intermediate stage, followed by the +Z_{DR} column collapse, resulting in an average behavior for this layer. The spreading of the ρ_{HV} (Figure 13d, light gray boxes) for low values is noteworthy and is only

observed at the time of the first CG flash, indicating that a mixture of supercooled raindrops and freezing hydrometers is predominant at this time. On the other hand, in the mixed 2 layer (Figures 13b and 13c, dark gray boxes), there is evidence for the freezing of large concentrations of supercooled raindrops, indicated by a narrowing of the Z_{DR} distribution and by Z_{DR} approaching near-to-zero values, while the K_{DP} distribution reached negative values before the time of the CG flash. In the glaciated layer (Figures 13c, blue boxes) the K_{DP} distribution was narrow and predominantly negative (down to $-0.6° \, \text{km}^{-1}$), and Z_H was as strong as 55 dBZ at the time of the first IC and CG flashes. This demonstrates that a large concentration of ice crystals with different sizes, such as plates or columns, was oriented vertically by a strong electric field. Indeed, the existence of columnar crystals between $-40°$ and $-70°C$ is the likely cause of the negative Z_{DR} and K_{DP}, which was suggested by an actual ice habit diagram [*Bailey and Hallett*, 2009]. However, some large positive and outlier values ($>$+1.5 dB) for Z_{DR} in the glaciated layer could in part be associated with cross-coupling effects of the horizontally and vertically transmitted waves caused by vertically oriented ice crystals in the mixed layer [*Hubbert et al.*, 2014b]. The subtle differences in terms of polarimetric variables between the time of the first IC and CG flashes in the mixed and glaciated layers are often a result of the initial IC and CG flashes belonging to the same radar volume scan.

To build a description of the average thunderstorm life cycle, the mean polarimetric variables were computed for the different cloud altitude ranges (Figure 14). In the warm layer (Figure 14a), an increase in Z_H, Z_{DR}, and K_{DP} was observed up to the time of the first IC flash (from #1Echo to #1CG), suggesting the formation of large raindrops by this time. The average ρ_{HV} in the warm layer decreased from the intermediate stage to the time of the first CG flash, suggesting the existence of melting graupel or a mixture of melting graupel and large raindrops in this layer. In the mixed 1 layer (Figure 14b), K_{DP} and Z_H dramatically increased, indicating the intrusion of supercooled raindrops in this layer, and at the same time ρ_{HV} decreased, indicating the mixing of hydrometeors as the thunderstorms evolve to the time of the first CG flash. In this layer (mixed 1 layer, Figure 14b), Z_{DR} shows the most notable behavior, an increase up to the intermediate stage, followed by a sharp decrease at the time of the first IC flash, indicating the freezing of supercooled raindrops aloft. In the mixed 2 layer (Figure 14c), the minimum Z_{DR} (+0.35 dB) and near-to-zero K_{DP} (+0.03 $°\, \text{km}^{-1}$) values are observed at the time of the first CG flash, indicating that graupel is likely forming via the accretion of supercooled cloud water in this layer.

In the glaciated layer, K_{DP} (Figure 14d) shows a striking characteristic; i.e., K_{DP} dramatically decreased to negative values during the thunderstorm evolution, suggesting rapid formation of ice particles and an electric field capable of orienting these hydrometeors vertically. Negative K_{DP} was documented in several works, such as *Caylor and Chandrasekar* [1996], *Tessendorf et al.* [2007], *Lang and Rutledge* [2008], *Dolan and Rutledge* [2009], and *Ventura et al.* [2013]. This result shows that the mean polarimetric information has typical signatures for each lifetime step of the thunderstorm electrification process. In the mixed 1 layer, both K_{DP} and Z_{DR} have remarkable signatures, while in the glaciated layer the K_{DP} behavior could be a good indicator of the time of the first CG flash.

This general statistical analysis considered only the polarimetric variables separately. Therefore, it is important to evaluate the relationships between the polarimetric variables simultaneously in the layers. The joint interpretation of two or more polarimetric variables from the same radar gate is much more effective and less prone to uncertainty and nonuniqueness than single parameter analysis. This procedure often provides the best clues for inferring cloud processes and precipitation properties. Figure 15 shows the scatterplots relating Z_H and Z_{DR} (a, c, e, and g) and Z_H and K_{DP} (b, d, f, and h) for the four predefined altitude ranges (i.e., warm, mixed 1, mixed 2, and glaciated layers) in the thunderstorms and for the four lifetime stages. The observations in the warm phase layer (Figures 15a and 15b) provide a confident identification of the main microphysical characteristics outlined in the previous analysis, indicating that the largest Z_H values (up to 67 dBZ) are associated with highly positive Z_{DR} (up to +6 dB) and K_{DP} (up to +6.5 $°\, \text{km}^{-1}$), especially near the time of the first CG flash. This finding demonstrates that the largest difference in the polarimetric fields remains confined to the regions of deeper and larger updrafts. Figure 15b also reveals that the largest Z_H values may have a large range of K_{DP} values from 0 to +6.5 $°\, \text{km}^{-1}$ in the warm layer. In part, these large K_{DP} values could be associated also with resonance effects [*Ryzhkov and Zrnic*, 2005] or nonuniform beam filling effects [*Gosset*, 2004]. If this effect is of second order, this large range K_{DP} (from 0 to 6.5$°\, \text{km}^{-1}$) with large Z_H ($>$ 40 dBZ) indicates the existence of different raindrop concentrations with a size distribution of raindrops skewed to large raindrops.
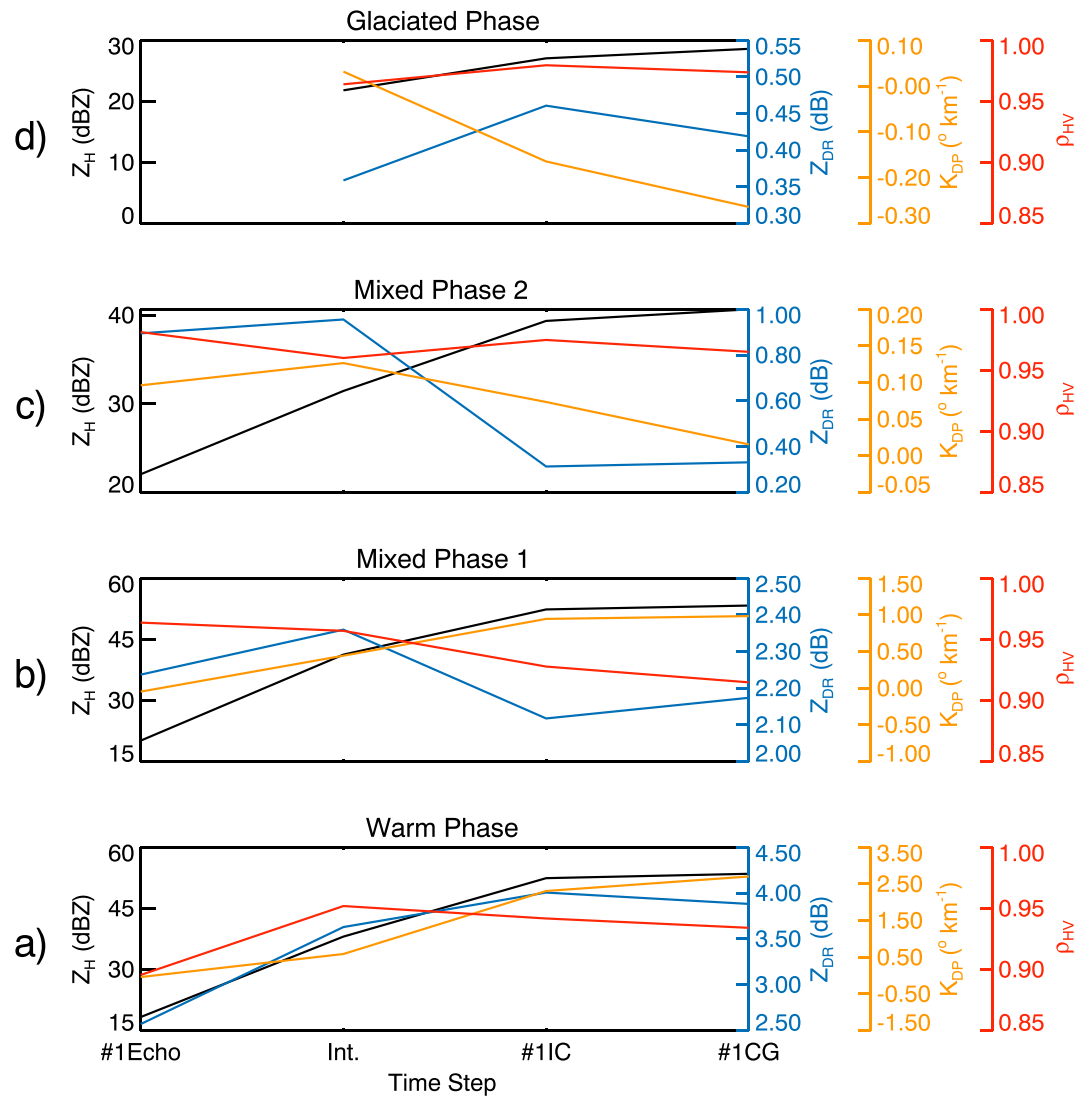
Figure 14. Mean values of Z_H (dBZ) (black line), Z_{DR} (dB) (blue line), K_{DP} (° km^{-1}) (orange line), and ρ_{HV} (red line) for the (a) warm, (b) mixed 1, (c) mixed 2, and (d) glaciated phase layers as a function of the four life cycle stages of thunderstorms: (i) #1Echo, (ii) Int.,(iii) #1CG, and (iv) #1CG.

In addition, note that the Z_H-K_{DP} relationship (Figure 15b) found here is very similar in shape to the traditional relationship between rain rate and reflectivity (Z_H-R). Both relationships (e.g., Z_H-K_{DP} and Z_H-R) are exponential and depend on the size distribution of raindrops; however, the Z_H-K_{DP} relationship depends also on total raindrop concentration and oblateness (or prolateness) of raindrops. As observed in this study the Z_H-K_{DP} relationship is influenced principally by large raindrops. An additional observation noted in the Figure 15b is that the strong rain rate associated with these large K_{DP} values is likely occurring close to time of the first CG flash in the cloud warm layer. The mixed 1 layer (Figures 15c and 15d) revealed a slightly positive relationship between Z_H, Z_{DR}, and K_{DP}. Notably, the initial stage of the mixed 1 layer was characterized by a Z_H above 20 dBZ with moderate Z_{DR} (up to +4.5 dB) and K_{DP} (up to +1.0° km^{-1}), indicating the formation of initial supercooled drops. On the other hand, weaker differences are noted between the time of the first IC and CG flash. However, we observed that the largest positive K_{DP} (+4.5° km^{-1}) and Z_H (60 dBZ) occur at the time of the first CG flash, suggesting an evolution from supercooled liquid water to frozen drops. Additionally, it is noted that a minimum in K_{DP} (down to −1° km^{-1}) was coincident with a near-to-zero Z_{DR} associated with strong Z_H (up to 60 dBZ), which is consistent with the presence of graupel and hail. The population of low Z_{DR} observed in the mixed 1 layer
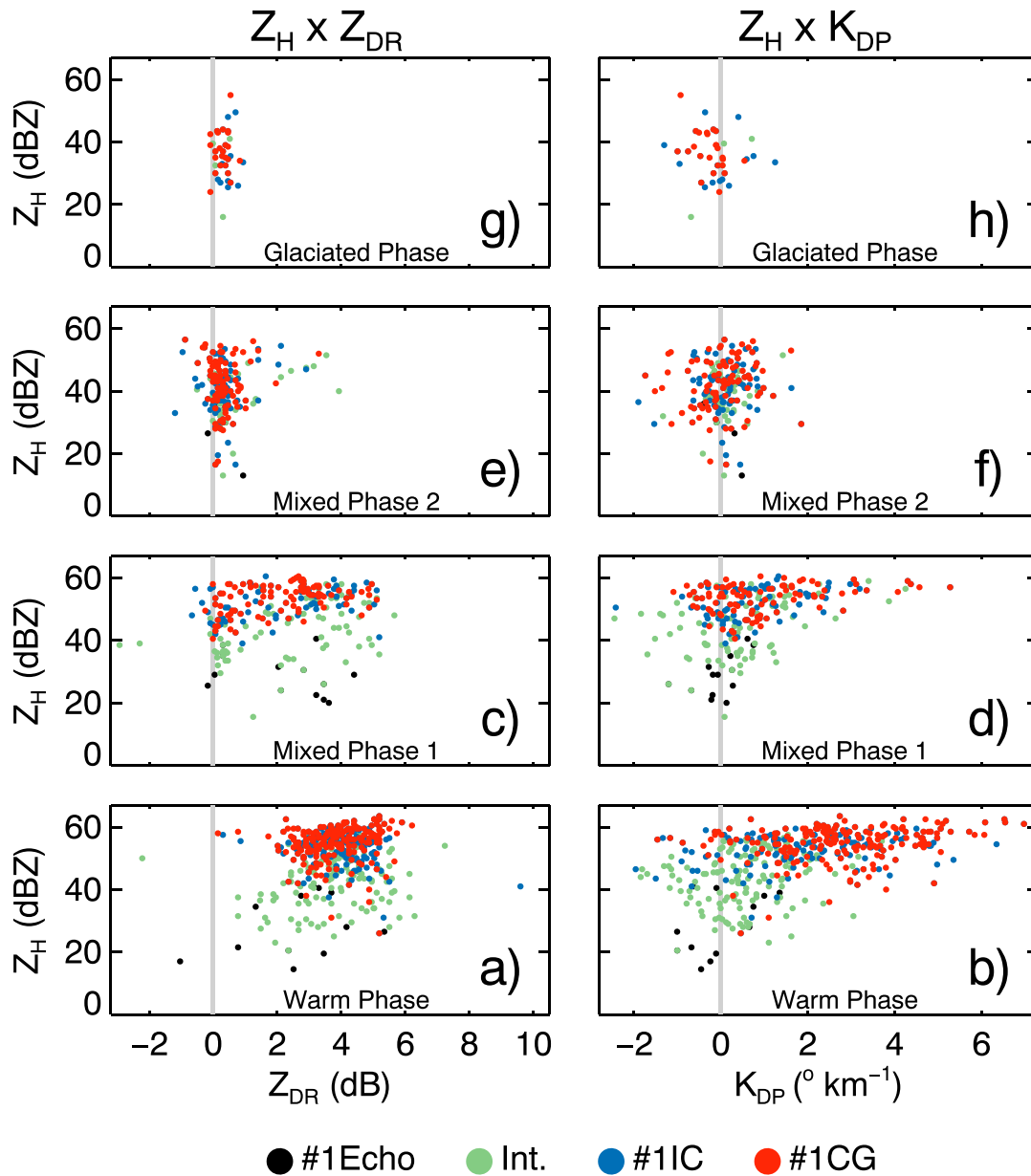
Figure 15. Scatterplots between (a, c, e, and g) Z_H (dBZ) and Z_{DR} (dB) and between (b, d, f, and h) Z_H (dBZ) and K_{DP} (° km^{-1}) for the warm (Figures 15a and 15b), mixed 1 (Figures 15c and 15d), mixed 2 (Figures 15e and 15f), and glaciated phase layers (Figures 15g and 15h) for the four life cycle stages of thunderstorms: (i) #1Echo (black dots), (ii) Int. (green dots), (iii) #1CG (blue dots), and (iv) #1CG (red dots).

could be related to small hail, lump and/or conical graupel, or snow aggregates [*Aydin and Seliga*, 1984; *Evaristo et al.*, 2013]. As discussed by *Kumjian et al.* [2014], aggregates are probably not the primary target because they are formed in weaker updrafts that allow larger crystals to fall and collect smaller ice crystals. In this study, it is evident that the first flash occurs in a region with deeper updrafts, which are favorable to the formation of hail and graupel promoting the noninductive cloud electrification mechanism.

Notably, in the mixed 2 layer (Figures 15e and 15f), near-to-zero Z_{DR} was predominant and associated with Z_H from 20 to 55 dBZ and negative K_{DP} (down to -2° km^{-1}) at the time of the first CG flash. This demonstrates that hail and graupel are dominant signatures in this layer. In contrast, negative K_{DP} (down to -1° km^{-1}) with moderate Z_H (from 25 to 45 dBZ) are predominant signatures in the glaciated layer (Figures 15g and 15h). Larger Z_H (35–45 dBZ) values with negative K_{DP} (down to -1° km^{-1}) are consistent with signatures from conical graupel [i.e., *Evaristo et al.*, 2013; *Bringi et al.*, 2016]. However, since these reflectivity values
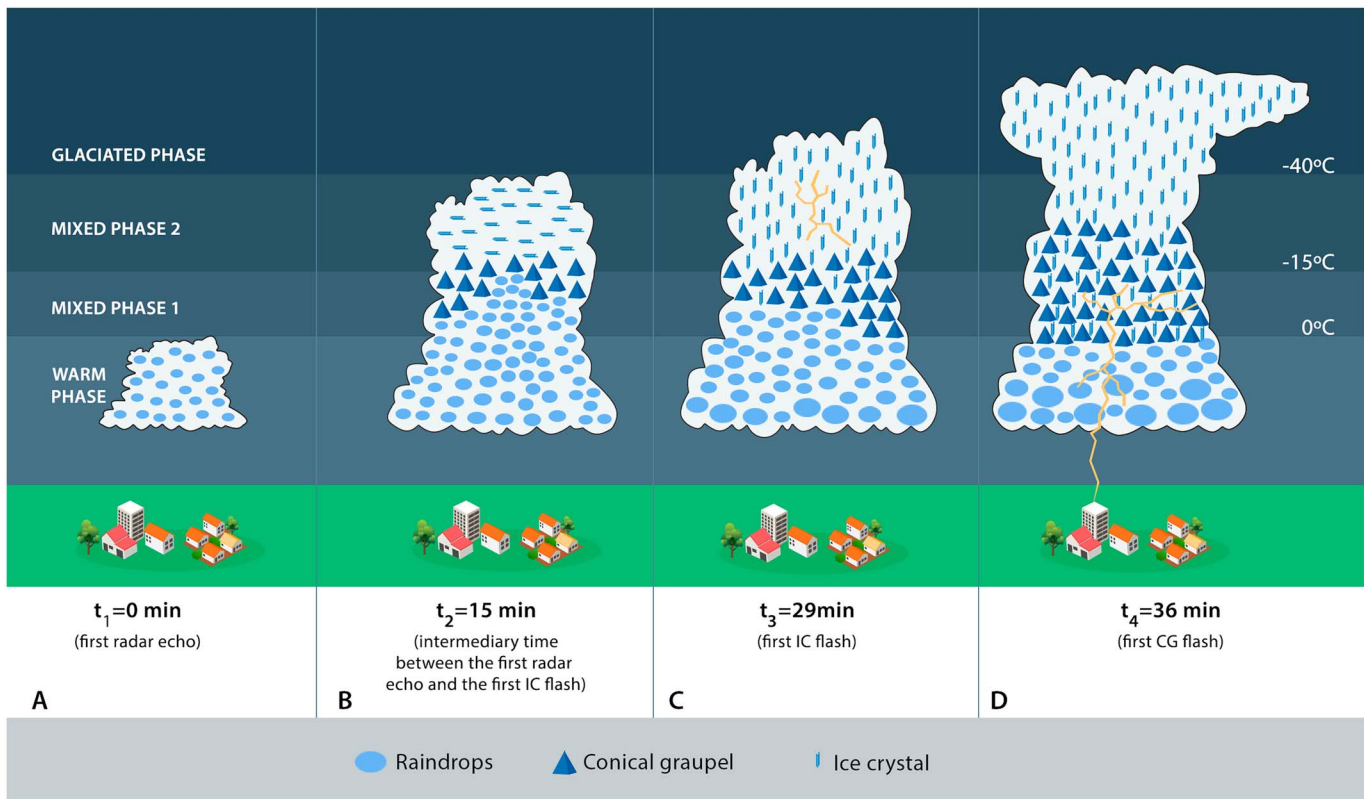
Figure 16. Conceptual model of the thunderstorm electrification life cycle. Here is shown the evolution from the first radar echo up to the time of the first cloud-to-ground flash: (a) the time of the first radar echo (#1Echo, $t_1 = 0$ min), (b) the intermediate time between the first echo radar and the first intracloud lightning flash (Int., $t_2 = 15$ min), (c) the time of the first intracloud lightning flash (#1IC, $t_3 = 29$ min), and (d) the time of the first cloud-to-ground lightning flash (#1CG, $t_4 = 36$ min).

represent the maximum Z_H extracted in each elevation angle, this approach is masking some of the strongest negative K_{DP} and Z_{DR} values associated with vertical ice crystals. Consistent with this picture, the vertical cross sections (Figures 4, 7, and 10) showed that both negative K_{DP} ($-0.3° \text{ km}^{-1}$) and Z_{DR} (-2 dB) values are more prevalent at low reflectivity (20–30 dBZ) than at higher values in the region above the $-40°C$ level in the cloud. Therefore, although conical graupel probably is present (dominating the Z_H signatures and which may be masking the signatures from vertical ice crystals), the existence of vertically aligned ice crystals by strong electric field is prevalent and notable when considering the whole glaciated layer. As suggested by *Weinheimer and Few* [1987] and by an actual ice habit diagram in *Bailey and Hallett* [2009], these ice particles are likely plates or columns, although columnar crystals between $-40°$ and $-70°C$ are much more likely to align than plate-like crystals.

6. Discussion and Conclusions

This study describes the polarimetric characteristics as a function of the life cycle in different cloud layers to estimate thunderstorm microphysical properties from the time of the first radar echo until the production of the first IC and CG lightning flashes. Observations of 46 thunderstorms during the 2011/2012 spring-summer in Southeast Brazil with an XPOL radar and two- and three-dimensional Lightning Location Systems demonstrated the key parameters in different layers related to the initial electrification process in these thunderstorms.

A discussion of three case studies in detail revealed the main characteristics of the thunderstorms life cycle. Time-height plots and vertical cross sections of the thunderstorm lifecycle evolution were the basis for this analysis. The study cases showed highly positive Z_{DR} and K_{DP} columns extending up to the $-15°C$ isotherm prior to the first IC and CG flashes, suggesting a lofting of supercooled raindrops by strong updrafts feeding the production of hail or conical graupel. We observed that these $+Z_{DR}$ columns extended to higher levels,

with a region aloft characterized by a negative Z_{DR} signature, indicating the likely existence of highly charged ice and graupel hydrometeors. The first IC flash was observed at the top of the $+Z_{DR}$ column in the central dipole region close to the $-16°C$ (7 km) isotherm, followed by the first CG flash observed below this layer. The thunderstorm configuration at this time showed a strong heterogeneous horizontal distribution of hydrometeors. These characteristics were clearly observed on a case-by-case basis as well as in the statistical analysis. There was notably a minimum ρ_{HV} on the boundary of the positive Z_{DR} and negative Z_{DR} regions (Figures 4, 7, and 10) indicating a freezing zone, as a result of the mixture of ice and liquid particles. This result is consistent with other observations of reduced ρ_{HV} or even enhanced linear depolarization ratio (LDR) near the tops of $+Z_{DR}$ columns [*Bringi et al.*, 1997; *Hubbert et al.*, 1998; *Smith et al.*, 1999; *Kumjian et al.*, 2014; *Snyder et al.*, 2015]. *Hubbert et al.* [1998] documented through polarimetric radar measurements that regions with low ρ_{HV} (0.94–0.96) were coincident with regions of strong LDR (≥ -22 dB) and strong reflectivity (40–50 dBZ) at the top of the $+Z_{DR}$ column, consistent with a mixture of supercooled drops, partially frozen drops, and asymmetric graupel. In addition, *Smith et al.* [1999] presented comparisons between T-28 aircraft measurements and LDR in 3 cm radar observations in mixed-phase regions that showed the presence of drops in the process of freezing in regions with enhanced LDR signatures atop $+Z_{DR}$ columns.

The composite analysis considering all thunderstorms was largely consistent with the aforementioned cases. The statistical analysis of the 46 cases showed contrasts in the polarimetric signatures throughout the thunderstorm life cycle. The decrease of K_{DP} to negative values in the glaciated layer, from the time of the first development of the glaciated layer up to the time of the first CG flash, was clearly observed. This is likely related to the high concentrations of ice crystals, such as plates and columns, being vertically aligned by a strong electric field. The most important aspect of the observations going into this paper, which came originally from the visual examination of a large number of thunderstorms, is that an initial $+Z_{DR}$ (associated with supercooled raindrops) evolved to reduced Z_{DR} (and even negative values) in the mixed 1 layer before and during the time of the initial lightning, suggesting an evolution from supercooled raindrops to frozen particles and the formation of graupel.

Based on the above description, it is possible to develop a conceptual model of early electrification for isolated thunderstorms (Figure 16). This model illustrates the principal results found in this study with emphasis on the signatures of conical graupel in the mixed 1 layer and vertically aligned ice crystals due to the strong electric field in the glaciated layer from the first radar echo until the first CG lightning flash. The initial stage (Figure 16a) of thunderstorms is dominated by small raindrops growing by coalescence in the updrafts in the warm layer. If the upward air motion is sufficient, some of these raindrops may reach a height above the melting level and start to grow rapidly through collection of small droplets. The updraft intensifies and a well-defined $+Z_{DR}$ column (with mean value $+1$–2 dB) containing supercooled liquid raindrops is produced after a mean time of 15 min (Figure 16b). The eventual reduction in reflectivity of the $+Z_{DR}$ column is associated with the phase change in freezing raindrops and the attendant change in dielectric constant and is followed by the appearance of negative Z_{DR}. The existence of a mixture of supercooled drops and partially frozen drops, with a variety of shapes and dielectric constant, is likely responsible for the low ρ_{HV} observed at the top of the $+Z_{DR}$ columns and further supports the importance of mixed-phase hydrometeors in this region. *Atlas* [1966] and *Lhermitte and Williams* [1985] recognized this location as the "balance level" (6–7 km msl), where the particle mean terminal velocity is equal in magnitude to the upward air motion. This level is favorable to the formation of relatively large precipitation particles (graupel and small hail, associated with radar reflectivity in the range 45 and 50 dBZ) suspended in an updraft. By this time, the strong updrafts promote strong collision rate between the graupel and ice particles leading to an increase in the initial cloud electrification. After 29 min (Figure 16c), the conical graupel atop the $+Z_{DR}$ column in the updraft grow to sizes too large to be suspended, and accordingly, they begin to fall out. As they descend through the updrafts, more supercooled raindrops are collected and they are dragged down through the melting level. The descent of the conical graupel and the progressive freezing of the suspended supercooled raindrops mark the demise of the $+Z_{DR}$ column. The gravitational separation of charged ice crystals at higher levels and the oppositely charged graupel in lower levels promotes the formation of a strong electric field and the first IC flash is registered. Therefore, the $+Z_{DR}$ column shows a well-defined lifecycle consistent with plausible microphysics and suggests a potential for lightning nowcasting. The maximum intensity of the $+Z_{DR}$ column is reached before the first IC flash (~15 min before), followed by a weakening of the column at the moment of the first IC flash.

By the mean time around 36 min (Figure 16d) after the first radar echo, the strong electric field is sufficient to align the ice crystals close to the cloud top (above the −40°C isotherm) and the conical graupel are dominant between the melting layer up to −15°C. Ice crystals of many kinds (i.e., like columns and plates) are likely aligned vertically by the electric field in the glaciated layer, as suggested by *Weinheimer and Few* [1987]. At this time the strong electric field is intensified and the first CG flash is registered. The large negative K_{DP} in the glaciated layer and the decrease of Z_{DR} in the mixed 1 layer are systematic signatures before and during the time of the first CG flashes. Although these signatures are predominant in the mean behavior, it is important to note that positive and negative K_{DP} and Z_{DR} can exist simultaneously in time and space. This means that other kinds of hydrometers not mentioned in this study, such as hexagonal and lump graupel, and others kinds of horizontally oriented ice crystals due to gravity could coexist in these layers. However, this study shows that the existence of conical graupel and vertically aligned ice crystals is the predominant behavior during the initial electrification of incipient thunderstorms. In addition, the supercooled raindrop characteristic of the $+Z_{DR}$ column is a systematic feature observable before the first IC flash of a developing thunderstorm.

Despite the fact that Z_{DR} columns in the mixed phase and negative K_{DP} in the glaciated layer have been investigated in many studies in association with lightning occurrence, many of the details of their development and their relationship with initial lightning were not previously investigated in detail. Differently from previous studies, this work provides an extensive documentation of the first IC and CG lightning flashes (for 46 thunderstorms) using two- and three-dimensional Lightning Location Systems together with the time-resolved polarimetric observations for a special subset of storms with lower attenuation. These thunderstorms are very compact clouds (avoiding mesoscale effects), and this procedure enabled a simpler physical interpretation of early thunderstorm development and with reduced radar attenuation characteristic of radars operating at X-band. In addition, this study was carried out in another geographical location, in another hemisphere in the tropics, and the results presented in this work provide statistical confirmation of the previous studies but for isolated tropical clouds, giving additional information about the thunderstorm electrification life cycle.

Important practical applications are highlighted here. This model can be used to design a nowcasting tool. Changes in the size and height of the $+Z_{DR}$ column provide the potential for the formation of graupel and ice crystals, which are fundamental conditions for lightning occurrence. This feature can also be used to estimate thunderstorm strength and maturity, increasing the lead time for lightning nowcasting. Additionally, a systematic observation of conical graupel (negative Z_{DR}) in the mixed 1 layer and vertically oriented ice crystals (negative K_{DP}) in the upper levels of thunderstorms may provide helpful information concerning thunderstorm vigor and its lightning diagnostic. The description of the thunderstorm life cycle could also open new opportunities for microphysical and lightning parameterization in cloud-resolving models, as well as for the testing of numerical models that describe the life cycle. Future analyses should consider different meteorological contexts, the degree of baroclinicity, the effect of seasons, and different thunderstorm sizes to evaluate this conceptual model for isolated thunderstorms.

References

Albrecht, R. I., C. A. Morales, C. M. N. Iwabe, M. F. Saba, and H. Höller (2014), Using lightning mapper array to evaluate the lightning detection signatures at different technologies, paper presented at XV International Conference on Atmospheric Electricity, International Commission on Atmospheric Electricity, Norman, Okla.

Atlas, D. (1966), The balance level in convective storms, *J. Atmos. Sci.*, 23, 635–651, doi:10.1175/1520-0469(1966)023<0635:TBLICS>2.0.CO;2.

Aydin, K., and T. A. Seliga (1984), Radar polarimetric backscattering properties of conical graupel, *J. Atmos. Sci.*, 41, 1887–1892, doi:10.1175/1520-0469(1984)041<1887:RPBPOC>2.0.CO;2.

Bailey, J. C., R. J. Blakeslee, L. D. Carey, S. J. Goodman, S. D. Rudlosky, R. Albrecht, C. A. Morales, E. M. Anselmo, J. R. Neves, and D. E. Buechler (2014), São Paulo Lightning Mapping Array (SP-LMA): Network assessment and analyses for intercomparison studies and GOES-R proxy activities, paper presented at XV International Conference on Atmospheric Electricity, International Commission on Atmospheric Electricity, Norman, Okla.

Bailey, M. P., and J. Hallett (2009), A comprehensive habit diagram for atmospheric ice crystals: Confirmation from the laboratory, AIRS II, and other field studies, *J. Atmos. Sci.*, 66, 2888–2899, doi:10.1175/2009JAS2883.1.

Battan, L. J. (1973), *Radar Observation of the Atmosphere*, Univ. of Chicago Press, Chicago, Ill.

Blakeslee, R. J., J. C. Bailey, L. D. Carey, S. J. Goodman, S. D. Rudlosky, R. Albrecht, C. A. Morales, E. M. Anselmo, and J. R. Neves (2013), São Paulo Lightning Mapping Array (SP-LMA): Network assessment and analyses for intercomparison studies and GOES-R proxy activities, paper presented at CHUVA International Workshop, São Paulo, SP, Brazil.

Bringi, V. N., D. A. Burrows, and S. M. Menon (1991), Multiparameter radar and aircraft study of raindrop spectral evolution in warm-based clouds, *J. Appl. Meteorol.*, *30*, 853–880, doi:10.1175/1520-0450(1991)030,0853:MRAASO.2.0.CO;2.

Bringi, V. N., K. Knupp, A. Detwiler, L. Liu, I. J. Caylor, and R. A. Black (1997), Evolution of a Florida thunderstorm during the Convection and Precipitation/Electrification Experiment: The case of 9 August 1991, *Mon. Weather Rev.*, *125*, 2131–2160, doi:10.1175/1520-0493(1997) 125,2131:EOAFTD.2.0.CO;2.

Bringi, V. N., M. Thurai, and R. Hannesen (2007), Correcting the measured Z_{DR} for differential attenuation due to rain, in *Dual-Polarization Weather Radar Handbook*, pp. 51–54, Selex-SI Gematronik, Neuss, Germany.

Bringi, V., P. Kennedy, G. Huang, C. Kleinkort, M. Thurai, and B. Notaros (2016), Dual-polarized radar and surface observations of a winter graupel shower with negative Z_{DR} column, *J. Appl. Meteorol. Climatol.*, doi:10.1175/JAMC-D-16-0197.1.

Bruning, E. C., W. D. Rust, T. J. Schuur, D. R. MacGorman, P. R. Krehbiel, and W. Rison (2007), Electrical and polarimetric radar observations of a multicell storm in TELEX, *Mon. Weather Rev.*, *135*, 2525–2544, doi:10.1175/MWR3421.1.

Buechler, D. E., and S. J. Goodman (1990), Echo size and asymmetry: Impact on NEXRAD storm identification, *J. Appl. Meteorol.*, *29*, 962–969, doi:10.1175/1520-0450(1990)029<0962:ESAAIO>2.0.CO;2.

Carey, L. D., and S. A. Rutledge (1996), A multiparameter radar case study of the microphysical and kinematic evolution of a lightning pro-ducing storm, *Meteorol. Atmos. Phys.*, *59*, 33–64, doi:10.1007/BF01032000.

Carey, L. D., and S. A. Rutledge (1998), Electrical and multiparameter radar observations of a severe hailstorm, *J. Geophys. Res.*, *103*, 13,979–14,000, doi:10.1029/97JD02626.

Carey, L. D., and S. A. Rutledge (2000), The Relationship between precipitation and lightning in tropical island convection: A C-Band polarimetric radar study, *Mon. Weather Rev.*, *128*, 2687–2710, doi:10.1175/1520-0493(2000)128<2687:TRBPAL>2.0.CO;2.

Carey, L. D., W. A. Petersen, and W. K. Deierling (2009), Radar differential phase signatures of ice orientation for the prediction of lightning initiation and cessation, paper presented at 34th Conference on Radar Meteorology, Am. Meteorol. Soc., Williamsburg, Va.

Caylor, I. F., and V. Chandrasekar (1996), Time-varying ice crystal orientation in thunderstorms observed with multiparameter radar, *IEEE Trans. Geosci. Electron.*, *34*, 847–858, doi:10.1109/36.508402.

Caylor, I. J., and A. J. Illingworth (1987), Radar observations and modelling of warm rain initiation, *Q. J. R. Meteorol. Soc.*, *113*, 1171–1191, doi:10.1002/QJ.49711347806.

Chauzy, S., D. Raisonville, D. Hauser, and F. Roux (1980), Electrical and dynamical description of a frontal storm deduced from the LANDES 79 experiment, paper presented at Proc. Eighth Int. Conf. on Cloud Physics, Am. Meteorol. Soc., Clermont-Ferrand, Fr.

Conway, J. W., and D. S. Zrnić (1993), A study of embryo production and hail growth using dual-doppler and multiparameter radars, *Mon. Weather Rev.*, *121*, 2512–2528, doi:10.1175/1520-0493(1993)121<2511:ASOEPA>2.0.CO;2.

Dolan, B., and S. A. Rutledge (2009), A theory-based hydrometeor identification algorithm for X-band polarimetric radars, *J. Atmos. Oceanic Technol.*, *26*, 2071–2088, doi:10.1175/2009JTECHA1208.1.

Dye, J. E., W. P. Winn, J. J. Jones, and D. W. Breed (1989), The electrification of New Mexico thunderstorms. Part 1: Relationship between precipitation development and the onset of electrification, *J. Geophys. Res.*, *94*, 8643–8656, doi:10.1029/JD094iD06p08643.

Engholm, C. D., E. R. Williams, and R. M. Dole (1990), Meteorological and electrical conditions associated with positive cloud-to-ground lightning, *Mon. Weather Rev.*, *118*, 470–487, doi:10.1175/1520-0493(1990)118,0470:MAECAW.2.0.CO;2.

Evaristo, R., T. M. Bals-Elsholz, E. R. Williams, D. J. Smalley, M. F. Donovan, and A. Fenn (2013), Relationship of graupel shape to differential reflectivity: Theory and observations, paper presented at 93rd Am. Meteorol. Soc. Annual Meeting, Am. Meteorol. Soc., Austin, Tex.

Foster, T. C., and J. Hallett (2002), The alignment of ice crystals in changing electric fields, *Atmos. Res.*, *62*, 149–169, doi:10.1016/S0169-8095 (02)00008-X.

Goodman, S. J., D. E. Buechler, P. D. Wright, and W. D. Rust (1988), Lightning and precipitation history of a microburst-producing storm, *Geophys. Res. Lett.*, *15*, 1185–1188, doi:10.1029/GL015i011p01185.

Goodman, S. J., et al. (2005), The North Alabama Lightning Mapping Array: Recent severe storm observations and future prospects, *Atmos. Res.*, *76*(1–4), 423–437, doi:10.1016/j.atmosres.2004.11.035.

Gosset, M. (2004), Effect of nonuniform beam filling on the propagation of radar signals at X-band frequencies. Part II: Examination of dif-ferential phase shift, *J. Atmos. Oceanic Technol.*, *21*, 358–367, doi:10.1175/1520-0426(2004)021<0358:EONBFO>2.0.CO;2.

Gremillion, M. S., and R. E. Orville (1999), Thunderstorm characteristics of cloud-to-ground lightning at the Kennedy Space Center, Florida: A study of lightning initiation signatures as indicated by the WSR-88D, *Weather Forecasting*, *14*, 640–649, doi:10.1175/1520-0434(1999) 014<0640:TCOCTG>2.0.CO;2.

Hall, M. P. M., S. M. Cherry, J. W. F. Goddard, and G. R. Kennedy (1980), Rain drop sizes and rainfall rate measured by dual-polarization radar, *Nature*, *285*, 195–198, doi:10.1038/285195a0.

Hall, M. P. M., J. W. F. Goddard, and S. M. Cherry (1984), Identification of hydrometeors and other targets by dual-polarization radar, *Radio Sci.*, *19*, 32–140, doi:10.1029/RS019i001p00132.

Hallett, J., and S. C. Mossop (1974), Production of secondary ice particles during the riming process, *Nature*, *249*, 26–28, doi:10.1038/249026a0.

Harris, R. J., J. R. Mecikalski, W. M. Mackenzie Jr., P. A. Durkee, and K. E. Nielsen (2010), The definition of GOES infrared lightning initiation interest fields, *J. Appl. Meteorol. Climatol.*, *49*, 2527–2543, doi:10.1175/2010JAMC2575.1.

Herzegh, P. H., and A. R. Jameson (1992), Observing precipitation through dual-polarization radar measurements, *Bull. Am. Meteorol. Soc.*, *73*, 1365–1374, doi:10.1175/1520-0477(1992)073<1365:OPTDPR>2.0.CO;2.

Homeyer, C. R., and M. R. Kumjian (2015), Microphysical characteristics of overshooting convection from polarimetric radar observations, *J. Atmos. Sci.*, *72*, 870–891, doi:10.1175/JAS-D-13-0388.1.

Hondl, K. D., and M. D. Eilts (1994), Doppler radar signatures of developing thunderstorms and their potential to indicate the onset of cloud-to-ground lightning, *Mon. Weather Rev.*, *122*, 1818–1836, doi:10.1175/1520-0493(1994)122<1818:DRSODT>2.0.CO;2.

Hubbert, J. C., S. M. Ellis, W. -Y. Chang, and M. Dixon (2014a), Modeling and interpretation of S-band ice crystal depolarization signatures from data obtained by simultaneously transmitting horizontally and vertically polarized fields, *J. Appl. Meteorol. Climatol.*, *53*, 1659–1677, doi:10.1175/JAMC-D-13-0158.1.

Hubbert, J. C., S. M. Ellis, W.-Y. Chang, and Y.-C. Liou (2014b), X-band polarimetric observations of cross coupling in the ice phase of con-vective storms in Taiwan, *J. Appl. Meteorol.*, *53*, 1678–1695, doi:10.1175/JAMC-D-13-0360.1.

Hubbert, J., and V. N. Bringi (1995), An iterative filtering technique for the analysis of copolar differential phase and dual-frequency radar measurements, *J. Atmos. Oceanic Technol.*, *12*, 643–648, doi:10.1175/1520-0426(1995)012<0643:AIFTFT>2.0.CO;2.

Hubbert, J., V. N. Bringi, L. D. Carey, and S. Bolen (1998), CSU-CHILL polarimetric radar measurements from a severe hail storm in eastern Colorado, *J. Appl. Meteorol.*, *37*, 749–775, doi:10.1175/1520-450(1998)037<0749:CCPRMF>2.0.CO;2.

Illingworth, A. J., J. W. F. Goddard, and S. M. Cherry (1987), Polarization radar studies of precipitation development in convective storms, *Q. J. R. Meteorol. Soc.*, *113*, 469–489, doi:10.1002/QJ.49711347604.

Jameson, A. R., M. J. Murphy, and E. P. Krider (1996), Multiple-parameter radar observations of isolated Florida thunderstorms during the onset of electrification, *J. Appl. Meteorol.*, *35*, 343–354, doi:10.1175/1520-0450(1996)035<0343:MPROOI>2.0.CO;2.

Krehbiel, P. R. (1986), The electrical structure of thunderstorms, in *The Earth's Electrical Environment*, pp. 90–113, Natl. Acad. Press, Washington, D. C.

Krehbiel, P., T. Chen, S. McCrary, W. Rison, G. Gray, and M. Brook (1996), The use of dual channel circular-polarization radar observations for remotely sensing storm electrification, *Meteorol. Atmos. Phys.*, *59*, 65–82, doi:10.1007/BF01032001.

Kumjian, M. R., S. M. Ganson, and A. V. Ryzhkov (2012), Freezing of raindrops in deep convective updrafts: A microphysical and polarimetric model, *J. Atmos. Sci.*, *69*, 3471–3490, doi:10.1175/JAS-D-12-067.1.

Kumjian, M. R., A. P. Khain, N. Benmoshe, E. Ilotoviz, A. V. Ryzhkov, and V. T. J. Phillips (2014), The anatomy and physics of Z_{DR} columns: Investigating a polarimetric radar signature with a spectral bin microphysical model, *J. Appl. Meteorol. Climatol.*, *53*, 1820–1843, doi:10.1175/JAMC-D-13-0354.1.

Lang, T. J., and S. A. Rutledge (2008), Kinematic, microphysical, and electrical aspects of an asymmetric bow-echo mesoscale convective system observed during STEPS 2000, *J. Geophys. Res.*, *113*, D08213, doi:10.1029/2006JD007709.

Lhermitte, R., and E. Williams (1985), Thunderstorm electrification: A case study, *J. Geophys. Res.*, *90*, 6071–6078, doi:10.1029/JD090iD04p06071.

López, R. E., and J.-P. Aubagnac (1997), The lightning activity of a hailstorm as a function of changes in its microphysical characteristics inferred from polarimetric radar observations, *J. Geophys. Res.*, *102*, 16,799–16,813, doi:10.1029/97JD00645.

Lund, N. R., D. R. MacGorman, T. J. Schuur, M. I. Biggerstaff, and W. D. Rust (2009), Relationships between lightning location and polarimetric radar signatures in a small mesoscale convective system, *Mon. Weather Rev.*, *137*, 4151–4170, doi:10.1175/2009MWR2860.1.

MacGorman, D. R., et al. (2008), TELEX: The Thunderstorm Electrification and Lightning Experiment, *Bull. Am. Meteorol. Soc.*, *89*, 997–1013, doi:10.1175/2007BAMS2352.1.

Machado, L. A. T., et al. (2014), The CHUVA Project—How does convection vary across the Brazil?, *Bull. Am. Meteorol. Soc.*, doi:10.1175/BAMS-D-13-00084.1.

Marshall, T. C., M. Stolzenburg, P. R. Krehbiel, N. R. Lund, and C. R. Maggio (2009), Electrical evolution during the decay stage of New Mexico thunderstorms, *J. Geophys. Res.*, *114*, D02209, doi:10.1029/2008JD010637.

Mattos, E. V., and L. A. T. Machado (2011), Cloud-to-ground lightning and mesoscale convective systems, *Atmos. Res.*, *99*, 377–390, doi:10.1016/j.atmosres.2010.11.007.

Mattos, E. V., L. A. T. Machado, E. R. Williams, and R. I. Albrecht (2016), Polarimetric radar characteristics of storms with and without lightning activity, *J. Geophys. Res. Atmos.*, *121*, 14,201–14,220, doi:10.1002/2016JD025142.

McCaul, E. W., Jr., S. J. Goodman, K. M. LaCasse, and D. J. Cecil (2009), Forecasting lightning threat using cloud-resolving model simulations, *Weather Forecasting*, *24*, 709–729, doi:10.1175/2008WAF2222152.1.

Mecikalski, J. R., X. Li, L. D. Carey, E. W. Mccaul Jr., and T. A. Coleman (2013), Regional comparison of GOES cloud-top properties and radar characteristics in advance of first-flash lightning initiation, *Mon. Weather Rev.*, *141*, 55–74, doi:10.1175/MWR-D-12-00120.1.

Mecikalski, R. M., A. L. Bain, and L. D. Carey (2015), Radar and lightning observations of deep moist convection across Northern Alabama during DC3: 21 May 2012, *Mon. Weather Rev.*, *143*, 2774–2794, doi:10.1175/MWR-D-14-00250.1.

Metcalf, J. I. (1993), Radar observations of the effects of changing electric fields of thunderstorms, *Bull. Am. Meteorol. Soc.*, *74*, 1080–1083.

Metcalf, J. I. (1995), Radar observations of changing orientations of hydrometeors in thunderstorms, *J. Appl. Meteorol.*, *34*, 757–772, doi:10.1175/1520-0450(1995)034,0757:ROOCOO.2.0.CO;2.

Metcalf, J. I. (1997), Temporal and spatial variations of hydrometeor orientations in thunderstorms, *J. Appl. Meteorol.*, *36*, 315–321, doi:10.1175/1520-0450(1997)036,0315:TASVOH.2.0.CO;2.

Mosier, R. M., C. Schumacher, R. E. Orville, and L. D. Carey (2011), Radar nowcasting of cloud-to-ground lightning over Houston, Texas, *Weather Forecasting*, *26*, 199–212, doi:10.1175/2010WAF2222431.1.

Naccarato, K., A. C. V. Saraiva, M. M. F. Sabo, and C. Schumann (2012), First performance analysis of BrasilDat total lightning network in southeastern Brazil, paper presented at International Conference on Grounding and Earthing and 5th International Conference on Lightning Physics and Effects, Bonito, MS, Brazil.

Nelson, L. A. (2002), Synthesis of 3-dimensional lightning data and weather radar data to determine the distance that naturally occurring lightning travels from thunderstorms, MS thesis, Dep. of Engineering Physics, Air Force Inst. of Tech., Ohio.

Oue, M., M. R. Kumjian, Y. Lu, Z. Jiang, E. Clothiaux, J. Verlinde, and K. Aydin (2015), X-band polarimetric and Ka-band observations of a graupel-producing Arctic mixed-phase cloud, *J. Appl. Meteorol.*, *54*, 1335–1351, doi:10.1175/JAMC-D-14-0315.1.

Picca, J. C., M. R. Kumjian, and A. V. Ryzhkov (2010), Z_{DR} columns as a predictive tool for hail growth and storm evolution, paper presented at 25th Conf. on Severe Local Storms, Am. Meteorol. Soc., Denver.

Prigent, C., E. Defer, J. R. Pardo, C. Pearl, W. B. Rossow, and J. P. Pinty (2005), Relations of polarized scattering signatures observed by the TRMM Microwave instrument with electrical processes in cloud systems, *Geophys. Res. Lett.*, *32*, L04810, doi:10.1029/2004GL022225.

Ramachandran, R., A. Detwiler, J. Helsdon Jr., P. L. Smith, and V. N. Bringi (1996), Precipitation development and electrification in Florida thunderstorm cells during Convection and Precipitation/Electrification Project, *J. Geophys. Res.*, *101*, 1599–1619, doi:10.1029/95JD02931.

Reynolds, S. E., and M. Brook (1956), Correlation of the initial electric field and the radar echo in thunderstorms, *J. Meteorol.*, *13*, 376–380.

Reynolds, S. E., M. Brook, and M. F. Gourley (1957), Thunderstorm charge separation, *J. Meteorol.*, *14*, 426–436, doi:10.1175/1520-0469(1957)014<0426:TCS>2.0.CO;2.

Ryzhkov, A. V. (2007), The Impact of beam broadening on the quality of radar polarimetric data, *J. Atmos. Oceanic Technol.*, *24*, 729–744, doi:10.1175/JTECH2003.1.

Ryzhkov, A. V., and D. S. Zrnic (2005), Radar polarimetry at S, C, and X bands: Comparative analysis and operational implications, paper presented at 32nd Conference on Radar Meteorology, Am. Meteorol. Soc., Norman, Okla.

Ryzhkov, A. V., and D. S. Zrnic (2007), Depolarization in ice crystals and its effect on radar polarimetric measurements, *J. Atmos. Oceanic Technol.*, *24*, 1256–1267, doi:10.1175/JTECH2034.1.

Ryzhkov, A. V., V. B. Zhuravlyov, and N. A. Rybakova (1994), Preliminary results of X-band polarization radar studies of clouds and precipitation, *J. Atmos. Oceanic Technol.*, *11*, 132–139, doi:10.1175/1520-0426(1994)011,0132:PROXBP.2.0.CO;2.

Ryzhkov, A. V., S. E. Giangrande, and T. J. Schuur (2005), Rainfall estimation with a polarimetric prototype of WSR-88D, *J. Appl. Meteorol.*, *44*, 502–515, doi:10.1175/JAM2213.1.

Sakuragi, J., and T. Biscaro (2012), Determination of Z_{DR} offset and their impact in the hydrometeor classification, paper presented at XVII Brazilian Meteorological Conference, Brazilian Meteorol. Soc., Gramado, RS, Brazil.

Schneebeli, M., J. Sakuragi, T. Biscaro, C. F. Angelis, I. C. da Costa, C. Morales, L. Baldini, and L. A. T. Machado (2012), Polarimetric X-band weather radar measurements in the tropics: Radome and rain attenuation correction, *Atmos. Meas. Tech.*, *5*, 2183–2199, doi:10.5194/amt-5-2183-2012.

Seroka, G. N., R. E. Orville, and C. Schumacher (2012), Radar nowcasting of total lightning over the Kennedy Space Center, *Weather Forecasting*, *27*, 189–204, doi:10.1175/WAF-D-11-00035.1.

Smith, P. L., D. J. Musil, A. G. Detwiler, and R. Ramachandran (1999), Observations of mixed-phase precipitation within a CaPE thunderstorm, *J. Appl. Meteorol.*, *38*, 145–155, doi:10.1175/1520-0450(1999)038,0145:OOMPPW.2.0.CO;2.

Snyder, J. C., A. V. Ryzhkov, M. R. Kumjian, A. P. Khain, and J. Picca (2015), A Z_{DR} column detection algorithm to examine convective storm updrafts, *Weather Forecasting*, *30*, 1819–1844, doi:10.1175/WAF-D-15-0068.1.

Stolzenburg, M., T. C. Marshall, and P. R. Krehbiel (2015), Initial electrification to the first lightning flash in New Mexico thunderstorms, *J. Geophys. Res. Atmos.*, *120*, 11,253–11,276, doi:10.1002/2015JD023988.

Straka, J. M., D. S. Zrnić, and A. V. Ryzhkov (2000), Bulk hydrometeor classification and quantification using polarimetric radar data: Synthesis of relations, *J. Appl. Meteorol.*, *39*, 1341–1372, doi:10.1175/1520-0450(2000)039<1341:BHCAQU>2.0.CO;2.

Takahashi, T. (1978), Riming electrification as a charge generation mechanism in thunderstorms, *J. Atmos. Sci.*, *35*, 1536–1548, doi:10.1175/1520-0469(1978)035<1536:REAACG>2.0.CO;2.

Tessendorf, S. A., S. A. Rutledge, and K. C. Wiens (2007), Radar and lightning observations of normal and inverted polarity multicellular storms from STEPS, *Mon. Weather Rev.*, *135*, 3682–3706, doi:10.1175/2007MWR1954.1.

Testud, J., E. L. Erwan, E. Obligis, and M. Ali-Mehenni (2000), The rain profiling algorithm applied to polarimetric weather radar, *J. Atmos. Oceanic Technol.*, *17*, 332–356, doi:10.1175/1520-0426(2000)017<0332:TRPAAT>2.0.CO;2.

Tuttle, J. D., V. N. Bringi, H. D. Orville, and F. J. Kopp (1989), Multiparameter radar study of a microburst: Comparison with model results, *J. Atmos. Sci.*, *46*, 601–620, doi:10.1175/1520-0469(1989)046,0601:MRSOAM.2.0.CO;2.

Ventura, J. F., F. Honoré, and P. Tabary (2013), X-band polarimetric weather radar observations of a hailstorm, *J. Atmos. Oceanic Technol.*, *30*, 2143–2151, doi:10.1175/JTECH-D-12-00243.1.

Vincent, B. R., L. D. Carey, D. Schneider, K. Keeter, and R. Gonski (2004), Using WSR-88D reflectivity for the prediction of cloud-to-ground lightning: A central North Carolina study, *Nat. Weather Dig.*, *27*, 35–44.

Weinheimer, A. J., and A. A. Few (1987), The electric field alignment of ice particles in thunderstorms, *J. Geophys. Res.*, *92*, 14,833–14,844, doi:10.1029/JD092iD12p14833.

Wiens, K. C., S. A. Rutledge, and S. A. Tessendorf (2005), The 29 June 2000 supercell observed during STEPS. Part II: Lightning and charge structure, *J. Atmos. Sci.*, *62*, 4151–4177, doi:10.1175/JAS3615.1.

Williams, E. R., M. E. Weber, and R. E. Orville (1989), The relationship between lightning type and convective state of thunderclouds, *J. Geophys. Res.*, *94*(D11), 13,213–13,220, doi:10.1029/JD094iD11p13213.

Williams, E. R., et al. (2015), Measurements of differential reflectivity in snowstorms and warm season stratiform systems, *J. Appl. Meteorol. Climatol.*, *54*, 573–595, doi:10.1175/JAMC-D-14-0020.1.

Williams, E. R., E. V. Mattos, and L. A. T. Machado (2016), Stroke multiplicity and horizontal scale of negative charge regions in thunderclouds, *Geophys. Res. Lett.*, *43*, 5460–5466, doi:10.1002/2016GL068924.

Woodard, C. J., L. D. Carey, W. A. Petersen, and W. P. Roeder (2012), Operational utility of dual-polarization variables in lightning initiation forecasting, *Electron. J. Oper. Meteorol.*, *13*, 79–102.

Workman, E. J., and S. E. Reynolds (1949), Electrical activity as related to thunderstorm cell growth, *Bull. Am. Meteorol. Soc.*, *30*, 142–144.

Yang, Y. H., and P. King (2010), Investigating the potential of using radar echo reflectivity to nowcast cloud-to-ground lightning initiation over Southern Ontario, *Weather Forecasting*, *25*, 1235–1248, doi:10.1175/2010WAF2222387.1.

Zrnić, D. S., and A. V. Ryzhkov (1996), Advantages of rain measurements using specific differential phase, *J. Atmos. Oceanic Technol.*, *13*, 454–464, doi:10.1175/1520-0426(1996)013<0454:AORMUS>2.0.CO;2.